guanidinium salts significantly increases the PrP^{Sc} signal following immunofluorescence staining. Although the precise reason as to why PrP^{Sc}-specific detection is achieved by this pre-treatment remains unclear, this method is now used for the PrP^{Sc}-specific detection by immunofluorescence assay (IFA) and immunoelectron microscopy. Earlier studies reported that PrP^{Sc} is mainly localized at the plasma membrane, in secondary lysosomes and at a peri-nuclear Golgi region (Fournier *et al.*, 2000; Jeffrey *et al.*, 1992; McKinley *et al.*, 1991; Taraboulos *et al.*, 1990). However, recent immunocytochemical and immunoelectron microscopy studies showed that PrP^{Sc} is also localized to early endosomes (Veith *et al.*, 2009), late endosomes/multivesicular bodies (Arnold *et al.*, 1995; Pimpinelli *et al.*, 2005) and to endocytic recycling compartment (ERC) at peri-nuclear regions (Godsave *et al.*, 2008; Marijanovic *et al.*, 2009).

In spite of the large contribution of this method on elucidation of the localization of PrP^{Sc} in cells, the specificity

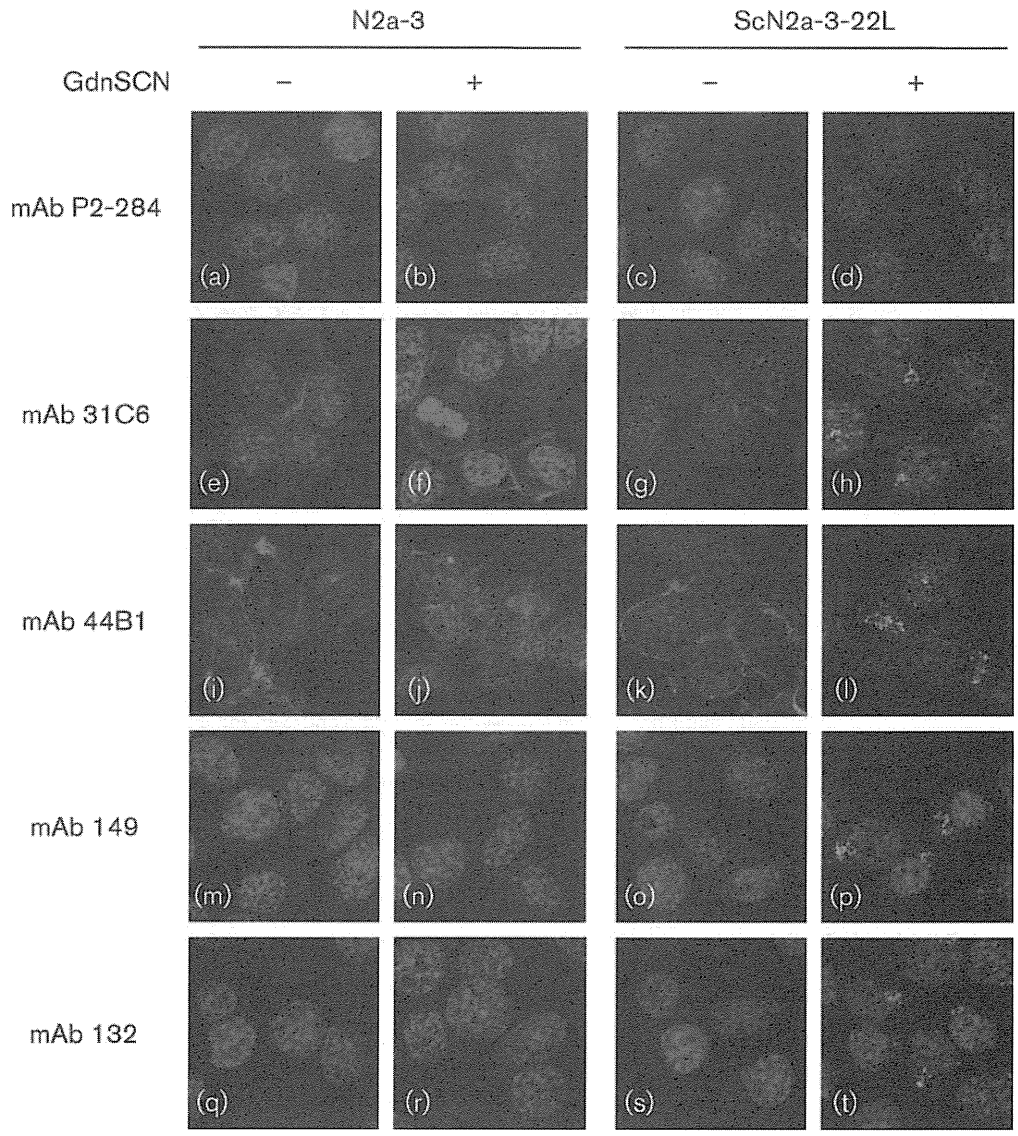

Fig. 1. Reactivity of mAbs to PrP in N2a-3 or ScN2a-3-22L cells with or without GdnSCN pre-treatment in IFA. N2a-3 cells and ScN2a-3-22L cells grown in chamber slides were fixed with 4 % paraformaldehyde and then permeabilized with 0.1 % saponin. The cells were treated with 5 M GdnSCN (b, d, f, h, j, l, n, p, r and t) or were left untreated (a, c, e, g, i, k, m, o, q and s), prior to antibody reaction. The anti-PrP mAbs 31C6 (e–h), 44B1 (i–l), 149 (m–p) and 132 (q–t) were used. The mAb P2-284 was used as a negative control (a–d). Cell nuclei were counterstained with DAPI. Merged images of PrP signals (green) and nuclei (blue) are shown. Nearly 100 % ScN2a-3-22L cells were positive for PrP^{Sc} in IFA using mAb 132.

of PrP^{Sc} detection by this method should be carefully re-evaluated. In fact, pre-treatment with guanidine hydrochloride (GdnHCl) does not prevent detection of PrP^{C} in uninfected cells (Taraboulos *et al.*, 1990; Veith *et al.*, 2009). In order to distinguish PrP^{Sc} from PrP^{C} by IFA, the detector gain or the exposure time needs to be adjusted to a level at which PrP^{C} signals are below the detection limit (Marijanovic *et al.*, 2009; Veith *et al.*, 2009). Alternatively, prior to pre-treatment with denaturants, proteinase K (PK) treatment is required to completely abolish PrP^{C} signals (Taraboulos *et al.*, 1990; Veith *et al.*, 2009). However, PK treatment affects cell architecture, which makes it difficult to finely analyse localization (unpublished observation). Resolution of these technical limitations will improve the quality of PrP^{Sc} detection in prion-infected cells. Taking these background studies into account, we first investigated the utility of various anti-PrP antibodies that recognize different epitopes on the PrP molecule for PrP^{Sc}-specific detection using IFA. We found that the mAb 132, which recognizes linear epitope consisting of mouse PrP aa 119–127 (Kim *et al.*, 2004b), the region adjacent to a hydrophobic amino acid sequence of PrP, AGAAAAGA, was the most suitable for this purpose. We therefore extensively analysed the localization of PrP^{Sc} in prion-infected cells using mAb 132. Our results suggest that PrP^{Sc} is trafficked through a cellular compartment at peri-nuclear regions along with the membrane trafficking machinery of the cells.

RESULTS

Specific detection of PrP^{Sc} in prion-infected cells by IFA

Pre-treatment of cells with denaturants such as guanidinium salts (Taraboulos *et al.*, 1990) and formic acid (Kristiansen *et al.*, 2005) prior to antibody reaction facilitates PrP^{Sc}-specific detection in prion-infected cells by IFA, although the precise mechanism by which this method distinguishes PrP^{Sc} from PrP^{C} remains unclear. However, one concern when using this method is that detection of PrP^{C} cannot be completely excluded as described below. In order to overcome this problem, we evaluated various anti-PrP mAbs for more accurate detection of PrP^{Sc} using IFA.

When N2a-3 cells, a subclone of mouse neuroblastoma Neuro2a cell line (Uryu *et al.*, 2007), without guanidine thiocyanate (GdnSCN) pre-treatment were stained with mAbs 31C6 or 44B1 that react strongly with PrP^{C} expressed on the cell surface, intense PrP^{C} signals were mainly detected at the plasma membrane (Fig. 1e, i). This membrane staining was not affected by GdnSCN pre-treatment (Fig. 1f, j). This result indicates that PrP^{C} was not removed from the cell surface by GdnSCN pre-treatment as described previously (Veith *et al.*, 2009). When N2a-3 cells persistently infected with the prion 22L strain (ScN2a-3-22L) without GdnSCN pre-treatment were stained with these mAbs, PrP signals were also detected at the cell surface similar to N2a-3 cells (Fig. 1g, k). However, staining of ScN2a-3-22L cells that were pre-treated with GdnSCN showed intense granular signals at the peri-nuclear regions (Fig. 1h, l). In addition to this peri-nuclear staining, weak signals at the cell surface were still detected (Fig. 1h, l), especially in areas where the cell density was high (data not shown). The presence of PrP signals at peri-nuclear regions of ScN2a-3-22L cells but not of N2a-3 cells pre-treated with GdnSCN, suggested that these peri-nuclear signals represent PrP^{Sc} as reported previously (Marijanovic *et al.*, 2009; Taraboulos *et al.*, 1990; Veith *et al.*, 2009). However, although signals at the plasma membrane of ScN2a-3-22L cells pre-treated with GdnSCN were much weaker than those of N2a-3 cells, the detection of PrP^{C} in N2a-3 cells after GdnSCN pre-treatment may raise a concern regarding distinction of PrP^{Sc} from PrP^{C}.

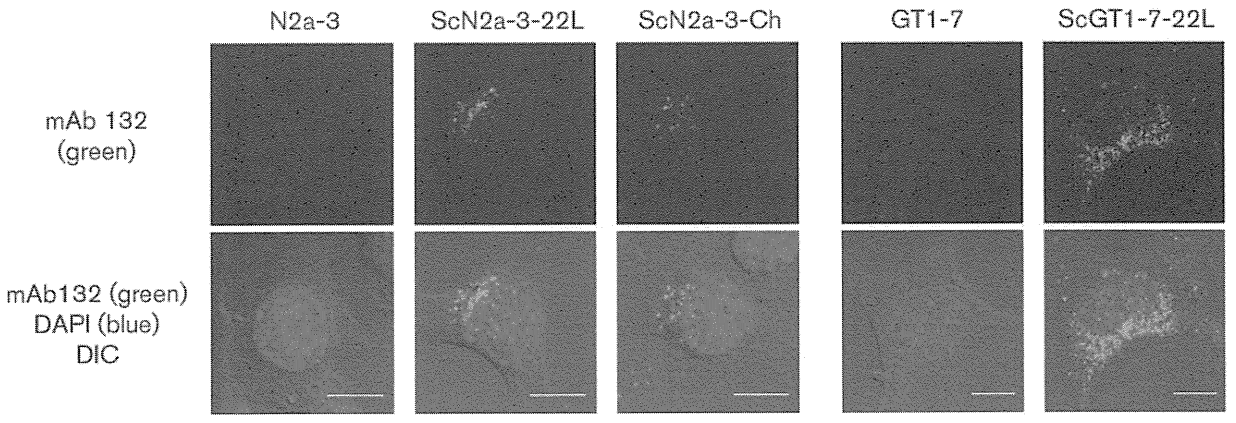

Fig. 2. PrP^{Sc}-specific detection in prion-infected cells using mAb 132. Non-infected N2a-3 and GT1-7 cells as well as ScN2a-3-22L, ScN2a-3-Ch and ScGT1-7-22L cells, were subjected to PrP^{Sc}-specific staining using mAb 132. The images in the upper panel show the PrP^{Sc} signals (green) and those in the bottom panel are differential interference contrast (DIC) images merged with PrP (mAb 132, green) and nuclear (DAPI, blue) fluorescent images. Bars, 10 μm.

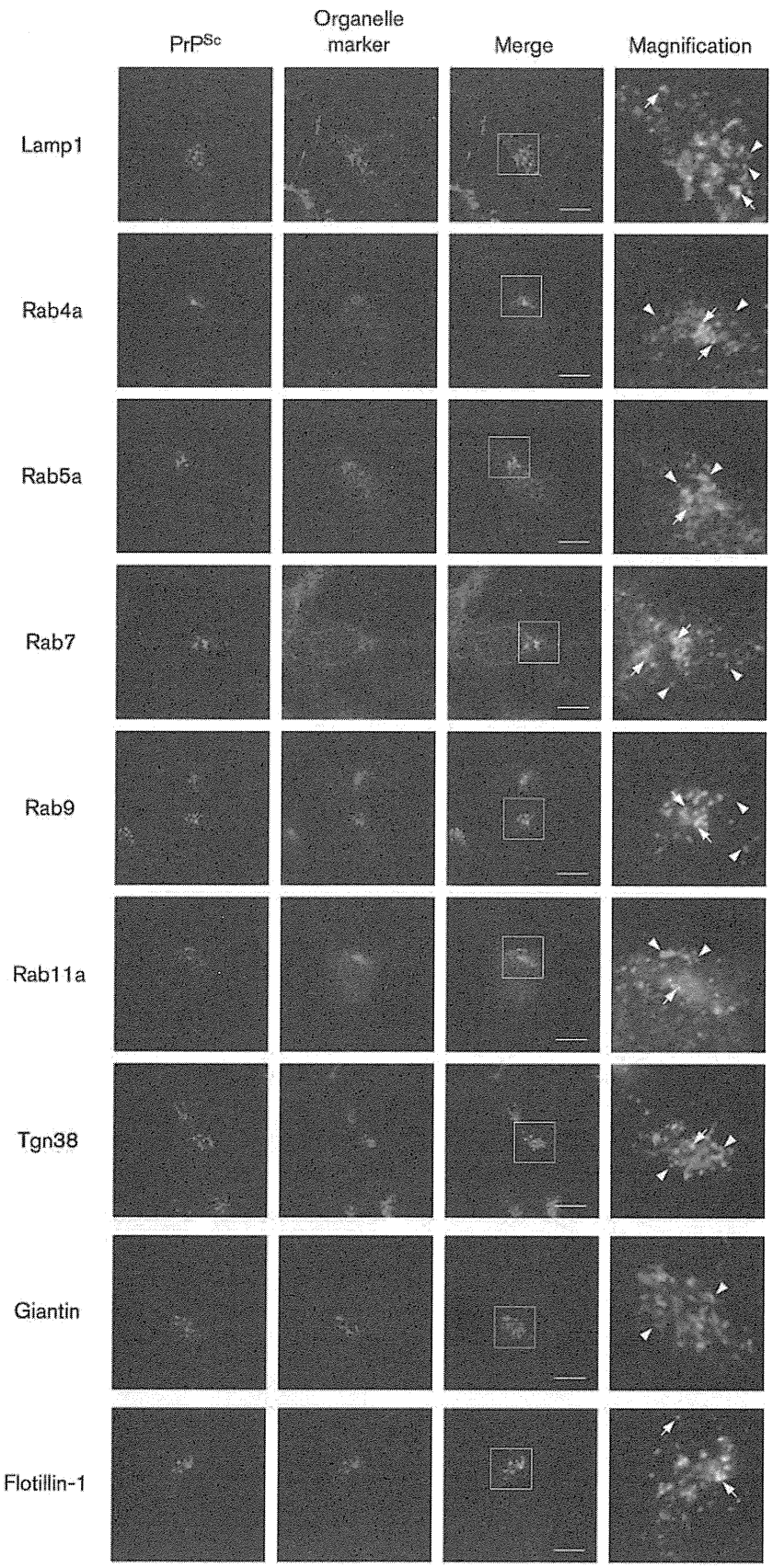

Fig. 3. Intracellular localization of PrP^{Sc}. ScN2a-3-22L cells were stained with the mAb 132 (PrP^{Sc}-specific staining, green) and antibodies against the organelle marker molecules indicated on the left (red). Images in the rightmost column show high magnification images of the boxed regions in the corresponding merged images. The arrows indicate representative examples of co-localization of PrP^{Sc} with the corresponding organelle markers (appear yellow), while the arrowheads indicate PrP^{Sc} that does not co-localize with the corresponding organelle markers (appear green). Bars, 10 μm.

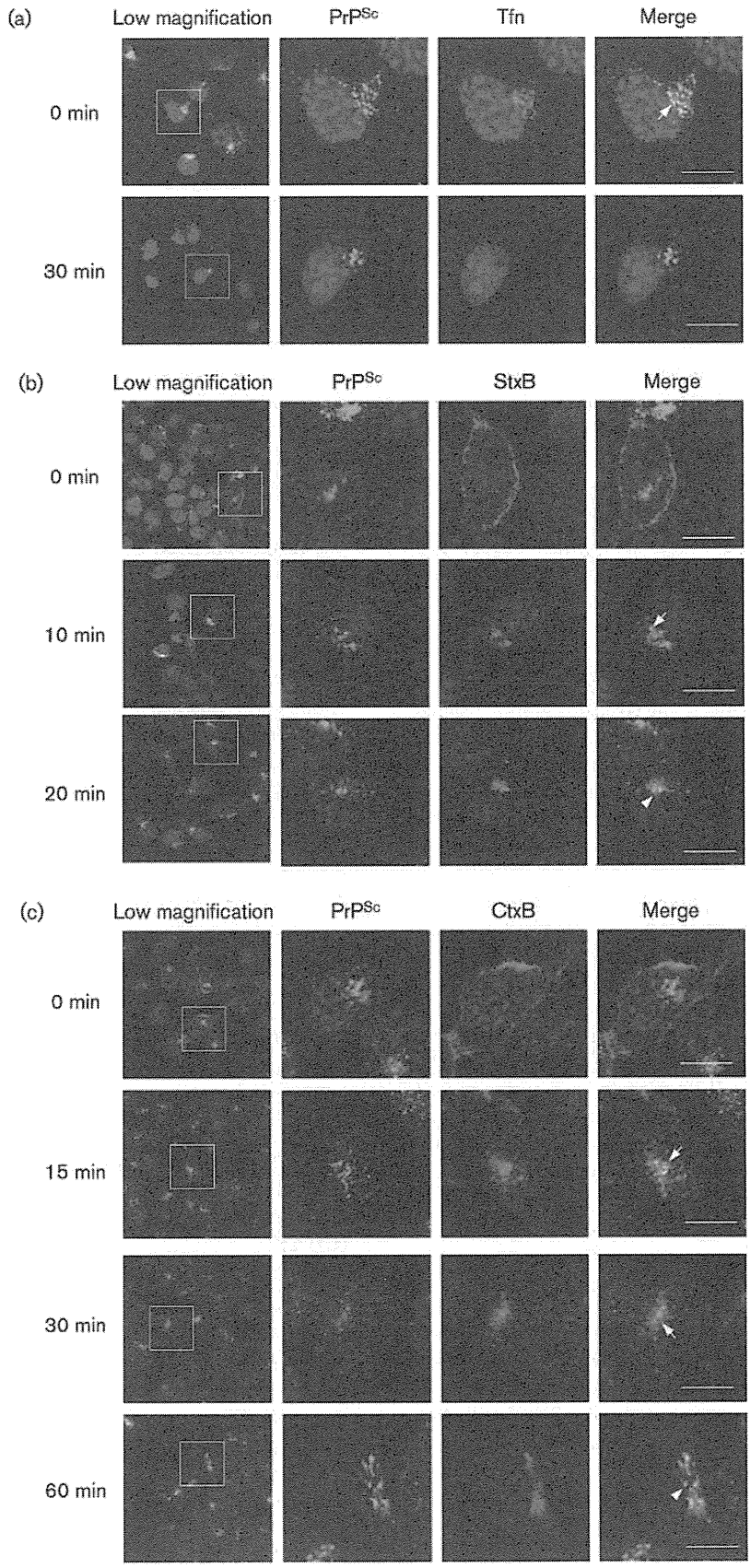
(a)
Low magnification
PrPSc
Tfn
Merge
0 min
30 min
(b)
Low magnification
PrPSc
StxB
Merge
0 min
10 min
20 min
(c)
Low magnification
PrPSc
CtxB
Merge
0 min
15 min
30 min
60 min

Fig. 4. Co-localization of PrP^{Sc} with Tfn, StxB and CtxB. (a) Localization of PrP^{Sc} and Tfn. ScN2a-3-22L cells were incubated with medium containing Alexa-Fluor-555-conjugated Tfn at 37 °C for 15 min (top, 0 min). Subsequently, the cells were cultured with Tfn-free fresh medium at 37 °C for 30 min (bottom, 30 min). All cells were fixed and subjected to PrP^{Sc}-specific staining using the mAb 132. The leftmost column shows a lower magnification of merged images of PrP^{Sc} (green), Tfn (red) and nuclei (blue). Individual and merged high magnification images of the boxed regions are shown on the right. The arrow indicates a representative example of the co-localization of PrP^{Sc} with Tfn. Bars, 10 μm. (b) Localization of PrP^{Sc} and StxB. ScN2a-3-22L cells were incubated with medium containing StxB at 4 °C for 60 min. After incubation, the cells were cultured with StxB-free fresh medium at 37 °C. The cells were fixed at the indicated time points and PrP^{Sc} and StxB were stained using the mAb 132 and anti-StxB rabbit polyclonal antibodies, respectively. The leftmost column shows a lower magnification of a merged image of PrP^{Sc} (green), StxB (red) and nuclei (blue). Individual and merged high magnification images of the boxed regions are shown on the right. The arrow indicates a representative example of co-localization of PrP^{Sc} with StxB, while the arrowhead indicates PrP^{Sc} that is not co-localized with StxB. Bars, 10 μm. (c) Localization of PrP^{Sc} and CtxB. ScN2a-3-22L cells were incubated with medium containing Alexa-Fluor-488-conjugated CtxB at 4 °C for 30 min. After incubation, the cells were cultured with CtxB-free fresh medium at 37 °C. The cells were fixed at each time point and PrP^{Sc} was stained using the mAb 132. The leftmost column shows a lower magnification of a merged image of PrP^{Sc} (green), CtxB (red) and nuclei (blue). Individual and merged high magnification images of the boxed regions are shown on the right. The arrows indicate representative examples of co-localization of PrP^{Sc} with CtxB, while the arrowhead indicates PrP^{Sc} that is not co-localized with CtxB. Bars, 10 μm.

We next tested mAbs 149 and 132, which display little reactivity with PrP^{C} on the surface of N2a cells by flow cytometric analysis (Kim *et al.*, 2004a). mAb 149 detected faint PrP signals in both N2a-3 and ScN2a-3-22L cells without GdnSCN pre-treatment (Fig. 1m, o). However, GdnSCN pre-treatment abolished the faint PrP^{C} signals detected in N2a-3 cells, but enhanced strong granular signals at peri-nuclear regions in ScN2a-3-22L cells (Fig. 1n, p). mAb 132 staining resulted in intense PrP signals at peri-nuclear regions in ScN2a-3-22L cells pre-treated with GdnSCN (Fig. 1t). Remarkably, this mAb detected little PrP^{C} in N2a-3 cells, regardless of the presence or absence of GdnSCN pre-treatment (Fig. 1q, r). Moreover, PrP signals in ScN2a-3-22L cells without GdnSCN pre-treatment appeared to be below the detection limit (Fig. 1s). We also verified the utility of mAb 132 for PrP^{Sc}-specific detection in different prion strains or cell lines (Fig. 2). Similar to ScN2a-3-22L cells, characteristic granular signals were detected in N2a-3 cells infected with the Chandler strain (ScN2a-3-Ch) and in GT1-7 cells persistently infected with the 22L strain (ScGT1-7-22L), but fluorescent PrP^{C} signals in uninfected cells remained at background level. Since hardly any PrP^{C} signal was detected in uninfected cells even after GdnSCN pre-treatment, mAb 132 is believed to enable more precise PrP^{Sc}-specific detection in IFA.

Intracellular localization of PrP^{Sc}

Since mAb 132 enables reliable PrP^{Sc}-specific detection, we used this mAb to analyse the intracellular localization of PrP^{Sc} in ScN2a-3-22L cells. Lamp1, a marker of late endosomes and/or lysosomes, has been reported to co-localize with PrP^{Sc} in prion-infected cells (Pimpinelli *et al.*, 2005). As expected, some PrP^{Sc} did co-localize with Lamp1 at peri-nuclear and peripheral regions of the cell (Fig. 3, arrows). However, PrP^{Sc} that was detected in a region extremely close to the nucleus did not co-localize with Lamp1 (Fig. 3, arrowheads).

We further analysed the co-localization of PrP^{Sc} with Rab GTPases that are known to be present in distinct organelles (Stenmark, 2009; Grant & Donaldson, 2009). Peri-nuclear PrP^{Sc} partially co-localized with Rab4a, a marker of early endosomes including rapid endocytic recycling endosomes; Rab5a, a marker of early endosomes; Rab7, a marker of late endosomes; Rab9, a marker of late endosomes involved in retrograde transport to the *trans*-Golgi network; and Rab11a, a marker of ERC (Fig. 3, arrows). In contrast to the co-localization of PrP^{Sc} with endosomal and lysosomal markers, only a small proportion of PrP^{Sc} co-localized with Tgn38, a marker of the *trans*-Golgi network. However, peri-nuclear PrP^{Sc} did not appear to co-localize with giantin, a marker of the *cis*/medial-Golgi (Fig. 3).

Flotillin-1 is a protein that is associated with lipid rafts and is known to be present at the plasma membrane, the *trans*-Golgi network and in endosomes, lysosomes and lipid droplets (Browman *et al.*, 2007). In contrast to the partial co-localization of PrP^{Sc} with the endosomal and lysosomal markers described above, a large proportion of PrP^{Sc} appeared to co-localize with flotillin-1 (Fig. 3).

PrP^{Sc} is localized to ERC in the intracellular transport pathway of transferrin (Tfn), Shiga toxin B subunit (StxB) and Cholera toxin B subunit (CtxB)

Recent ultrastructural and immunofluorescence studies have revealed that PrP^{Sc} is localized in endocytic compartments (Godsave *et al.*, 2008; Marijanovic *et al.*, 2009; Pimpinelli *et al.*, 2005; Veith *et al.*, 2009). Since PrP^{Sc} is often detected at the peri-nuclear regions very close to but not in the Golgi apparatus, of particular interest is the ERC that is located near the microtubule organizing centre and the Golgi apparatus that is involved in the recycling of membrane lipids and proteins (Grant & Donaldson, 2009). Therefore, to more precisely analyse juxtanuclear PrP^{Sc} localization, we used Tfn as a marker for the ERC. Tfn

binds the Tfn receptor that is internalized from the cell surface via clathrin-coated pits, is transported to early endosomes, and is then recycled back to the plasma membrane via the ERC (Maxfield & McGraw, 2004). When the cells were loaded with Alexa-Fluor-555-conjugated Tfn, Tfn was detected at the peri-nuclear regions 15 min after the initiation of uptake (time 0) and Tfn had almost disappeared 30 min after the removal of Tfn from the medium (Fig. 4a). Some of the juxtanuclear PrP^{Sc} did co-localize with internalized Tfn at peri-nuclear regions 15 min after Tfn loading, suggesting that the ERC is one of the compartments to which PrP^{Sc} localizes.

Flotillin-1 is reported to be involved in clathrin-independent endocytosis of StxB and CtxB (Glebov *et al.*, 2006; Lin & Guttman, 2010). StxB and CtxB are known to bind globotriaosylceramide and GM1 ganglioside, respectively, at cell surface and are transported from the plasma membrane to the *trans*-Golgi network via early endosomes and the ERC (Lieu & Gleeson, 2010; Nichols *et al.*, 2001). Since PrP^{Sc} clearly co-localized with flotillin-1 (Fig. 3), we further analysed the localization of PrP^{Sc} with StxB and CtxB. When cells were loaded with StxB at 4 °C and StxB was then internalized by transfer of the cells to 37 °C, StxB partly co-localized with PrP^{Sc} at the peri-nuclear region 10 min after initiation of internalization (Fig. 4b, arrow). However, co-localization of PrP^{Sc} with StxB was not so clear after further 10 min incubation (Fig. 4b, arrowhead). Similarly, co-localization of PrP^{Sc} with internalized CtxB was observed at the peri-nuclear regions 15 and 30 min after initiation of internalization, but co-localization was weaker after 60 min (Fig. 4c). At 15–30 min after initiation of internalization, CtxB at the peri-nuclear regions showed strong co-localization with Rab11a, but after 60 min, it co-localized more strongly with Tgn38. This result suggested that CtxB present at the peri-nuclear regions was mainly in the ERC at 15–30 min, and in the *trans*-Golgi network at 60 min after initiation of internalization (Fig. 5, 37 °C). These results indicate that PrP^{Sc} is present in the ERC, which is on the intracellular transport pathway of StxB and CtxB.

PrP^{Sc} dynamically cycles between peripheral and peri-nuclear regions in ScN2a-3-22L

The presence of PrP^{Sc} in various endocytic compartments, especially in the ERC through which Tfn, StxB and CtxB are transported, suggested that PrP^{Sc} is transported intracellularly by the membrane trafficking machinery of the cell, rather than being a permanent resident of these organelles. To address the association of PrP^{Sc} with the intracellular membrane trafficking machinery, we analysed the localization of PrP^{Sc} in ScN2a-3-22L cells that were incubated at 20 °C. Incubating cells at a low temperature ($\leqslant$20 °C) impairs the transport of Tfn or StxB from the plasma membrane to peri-nuclear regions (Mallard *et al.*, 1998; Ren *et al.*, 1998; Sipe *et al.*, 1991). We firstly confirmed that incubation of ScN2a-3-22L cells at 20 °C slowed down the transport of CtxB (Fig. 5) and StxB (data not shown). Following incubation at 37 °C, CtxB was concentrated at the peri-nuclear regions and co-localized with Rab11a within 15–30 min and with Tgn38 within 60 min, after initiation of its uptake. In contrast, CtxB did not co-localize with either Rab11a or Tga38 after 30 min of incubation at 20 °C, but co-localization with Rab11a could be observed 60 min after the start of incubation. In addition, some CtxB still remained at the plasma membrane 60 min after the incubation, indicating that the transport of CtxB from the plasma membrane to peri-nuclear regions had been slowed down. Under this condition, most of the PrP^{Sc} signals disappeared from the peri-nuclear regions and appeared at peripheral regions of the cells, including at the plasma membrane, within 1 h (Fig. 6a, 20 °C/1 h, arrowheads). After subsequent incubation for another hour, some of the PrP^{Sc} seemed to have redistributed to the peri-nuclear regions (Fig. 6a, 20 °C/2 h), following which, PrP^{Sc} gradually disappeared again from the peri-nuclear regions over the next 10 h of incubation. Indeed, following this incubation, the majority of PrP^{Sc} redistributed to the peripheral regions of the cells (Fig. 6a, 20 °C/12 h).

When ScN2a-3-22L cells that had been incubated at 20 °C for 12 h were transferred to 37 °C, peri-nuclear PrP^{Sc} signals appeared to increase and PrP^{Sc} signals at the peripheral regions appeared to decrease within 30 min of incubation (Fig. 6a, 37 °C/30 min). Interestingly, after an additional 30 min incubation at 37 °C, some of the PrP^{Sc} reappeared at the peripheral regions including the plasma membrane, although some PrP^{Sc} was still detected at the peri-nuclear regions (Fig. 6a, 37 °C/60 min, arrowheads). During subsequent 1 h incubation, PrP^{Sc} signals at the peripheral regions decreased again, and thereafter, signals of PrP^{Sc} at the peri-nuclear regions appeared to revert to the steady-state level (Fig. 6a, 37 °C/120 min). Little PrP^{C} was detected in N2a-3 cells throughout the experimental period (Fig. 6b), which means that both the peri-nuclear and the peripheral fluorescent signals represent PrP^{Sc}. In spite of the changes in the intracellular distribution of PrP^{Sc}, the amount of PrP-res, a representative of a protease-resistant form of PrP^{Sc}, was unchanged over the experimental period (Fig. 7). These results suggest that the dynamic changes in the distribution of PrP^{Sc} were not due to major differences in synthesis or degradation of PrP^{Sc} at specific regions of the cell, but were primarily due to the intracellular trafficking of PrP^{Sc} through the peri-nuclear regions.

DISCUSSION

Analysis of the intracellular localization of PrP^{Sc} is important for the understanding of the cellular mechanism of prion propagation. Taraboulos *et al.* (1990) showed that pre-treatment of prion-infected cells with GdnHCl enables PrP^{Sc}-specific detection using IFA. Although the mechanism of

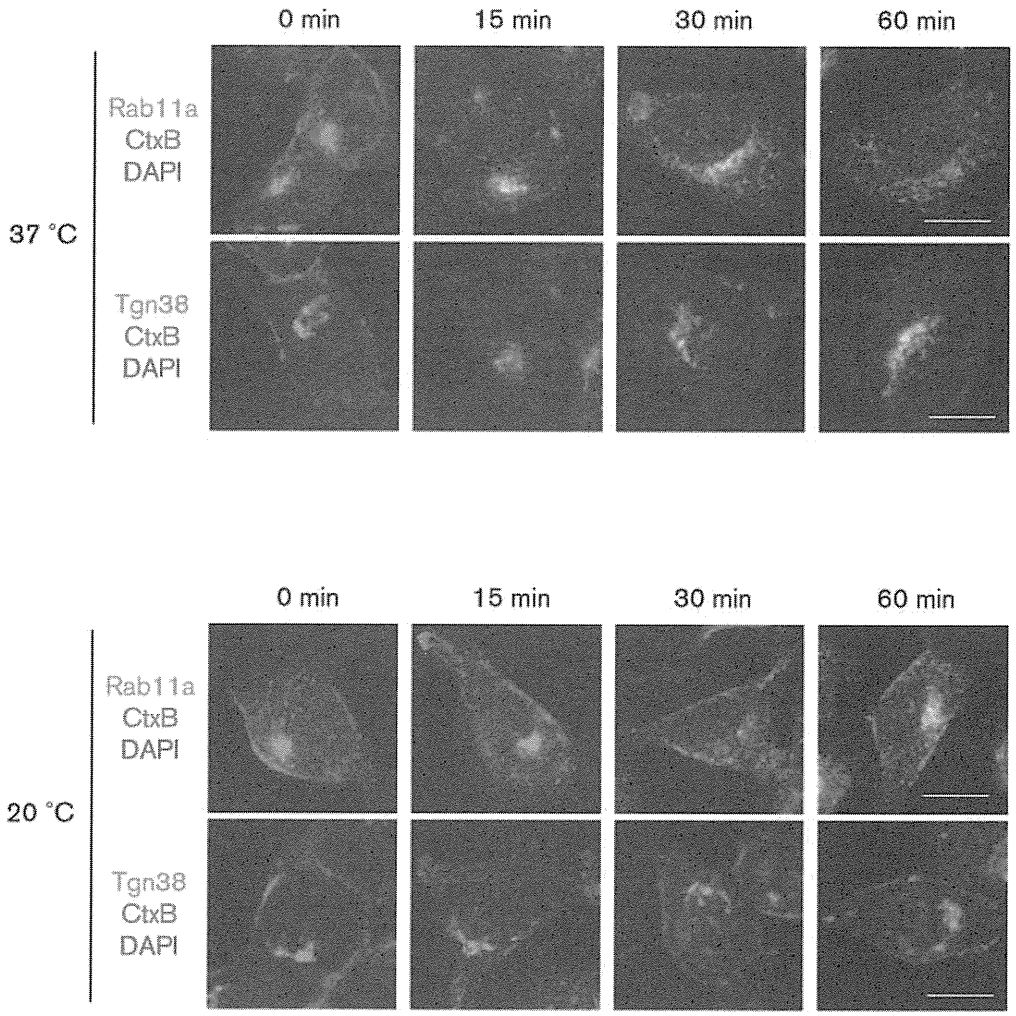

Fig. 5. Localization of CtxB with marker molecules. ScN2a-3-22L cells were incubated with medium containing Alexa-Fluor-488-conjugated CtxB at 4 °C for 30 min and the medium was then replaced with CtxB-free fresh medium. The cells were then incubated at 37 °C (top panel) or 20 °C (bottom panel) for up to 60 min. The cells were fixed at each time point and stained with anti-Rab11a or anti-Tgn38 rabbit polyclonal antibodies. Merged images of Rab11a or Tgn38 (green) with CtxB (red) and nuclei (blue) are shown. Bars, 10 μm

PrP^{Sc}-specific detection by pre-treatment of cells with chaotropic agents was unclear, this method has been used for the detection of PrP^{Sc} in cells and tissues (Marijanovic *et al.*, 2009; Pimpinelli *et al.*, 2005; Taraboulos *et al.*, 1990; Veith *et al.*, 2009). Treatment with denaturant facilitates exposure of cryptic epitopes of PrP^{Sc} (Taraboulos *et al.*, 1990). However, since GdnHCl treatment does not remove PrP^{C} from uninfected cells (Taraboulos *et al.*, 1990; Veith *et al.*, 2009; this study), detection of PrP^{C} signals would be expected because most of the antibodies against PrP molecules react not only with denatured PrP^{Sc} but also with denatured PrP^{C}. If signals from the denatured PrP^{Sc} are strong enough to distinguish them from PrP^{C}, then PrP^{Sc}-specific detection can be achieved by setting the threshold level just above the level of PrP^{C} signals by manipulation of the gain of detector, changing exposure time and so on. However, such adjustment will miss subtle details of the PrP^{Sc} signals. Therefore, further improvement of PrP^{Sc}-specific detection is still required for detailed characterization of the intracellular localization of PrP^{Sc}. To improve the specificity of PrP^{Sc} detection, we used mAb 132, which recognizes the epitope consisting of mouse PrP aa 119–127, adjacent to the hydrophobic amino acid sequence, AGAAAAGA (Gasset *et al.*, 1992). Since mAb 132 showed little reactivity with native PrP^{C} on the cell surface, the epitope for mAb 132 is thought to be buried inside the PrP^{C} molecule. Denaturation with GdnSCN was expected to expose the epitope for mAb 132 of PrP^{C}, but in fact, mAb 132 showed little reactivity with PrP^{C} in uninfected cells even after treatment with GdnSCN (Fig. 1). A reduction in PrP^{C}

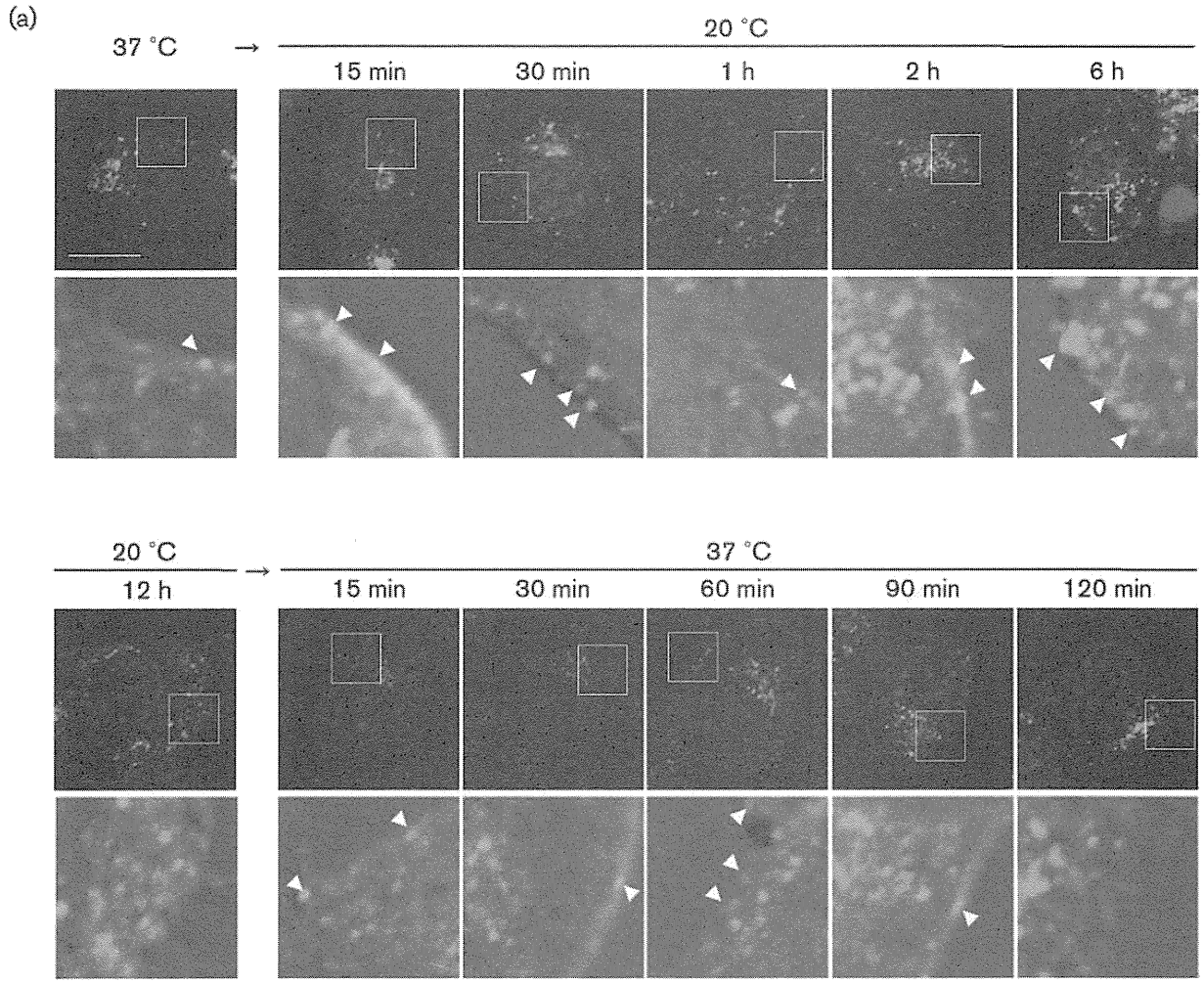
(a)
37 °C
20 °C
15 min
30 min
1 h
2 h
6 h
20 °C
12 h
37 °C
15 min
30 min
60 min
90 min
120 min

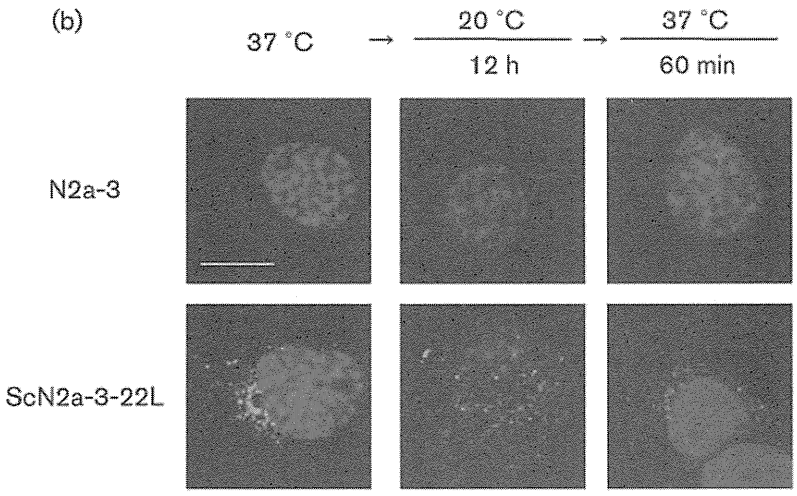
(b)
37 °C
20 °C
12 h
37 °C
60 min
N2a-3
ScN2a-3-22L

Fig. 6. Changes in the localization of PrP^{Sc} during incubation at 20 °C and subsequent incubation at 37 °C. (a) Temperature-dependent localization of PrP^{Sc} in ScN2a-3-22L cells. ScN2a-3-22L cells were grown on a chamber slide at 37 °C. The cells were then incubated at 20 °C for the indicated periods for up to 12 h. After 12 h incubation at 20 °C, the cells were incubated at 37 °C for up to 120 min as indicated. The cells were then fixed and subjected to PrP^{Sc}-specific staining using mAb 132. The upper panels show merged images of PrP^{Sc} (green) and nuclei (blue). The bottom panels show high magnification images of the boxed regions in the corresponding upper panels that were merged with a DIC image. The arrowheads point to representative examples of PrP^{Sc} signals at the cell surface. Bar, 10 μm. (b) Specificity of PrP^{Sc} staining. N2a-3 or ScN2a-3-22L cells cultured on a chamber slide at 37 °C were subsequently incubated at 20 °C for 12 h and then incubated at 37 °C for 60 min. These cells were fixed and subjected to PrP^{Sc}-specific staining using the mAb132. Bar, 10 μm.

labelling is an important factor for PrP^{Sc}-specific detection (Dron *et al.*, 2009). Indeed, this property of the mAb 132 allowed us to perform more precise PrP^{Sc} detection using IFA because the lack of, or trace PrP^{C} signal means that specific manipulation of the threshold setting during data acquisition can be minimized. Since mAb 132 reacts with denatured PrP^{C} and PrP^{Sc} in immunoblotting (Kim *et al.*, 2004b), the reason why mAb 132 cannot detect PrP^{C}, but can detect PrP^{Sc}, in cells pre-treated with GdnSCN remains unclear. However, one possible explanation is that the epitope for mAb 132 on PrP^{C} may not be exposed by the relatively short denaturation period (10 min exposure to GdnSCN). Alternatively, it is possible that once the epitope for mAb 132 on PrP^{C} has been exposed by denaturation with GdnSCN, PrP^{C} may quickly refold into a conformation that prevents access of mAb 132 to the epitope after the removal of GdnSCN. In contrast, PrP^{Sc} was detected in prion-infected cells after denaturation with GdnSCN (Fig. 1), indicating that the epitope-containing region of PrP^{Sc} molecules, unlike that of PrP^{C}, remained antibody-accessible. PrP^{Sc} has been reported to refold into a PrP^{C}-like form after strong denaturation with GdnHCl (Callahan *et al.*, 2001; Kocisko *et al.*, 1996). Given that short-term exposure of GdnSCN will not completely denature PrP^{Sc}, and that PrP^{Sc} exists as an oligomer, intermolecular interaction among neighbouring PrP molecules may disturb the refolding of denatured PrP^{Sc} and as a consequence, the epitope for mAb 132 on PrP^{Sc} molecule may remain accessible to the antibody.

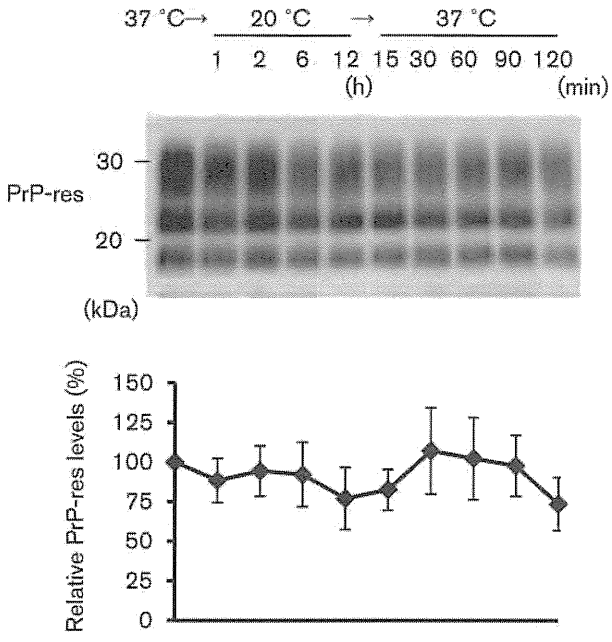

Fig. 7. Amount of PrP-res. ScN2a-3-22L cells cultured on 60 mm dishes at 37 °C were transferred to 20 °C and incubated for 1–12 h. After 12 h of incubation, the cells were incubated again at 37 °C for 15–120 min. The cells were lysed at the indicated time points and were subjected to immunoblotting for PrP-res detection. Sample volume equivalent to 4×10^{5} cells were loaded on each lane. A representative immunoblot image is shown on the top and the graph at the bottom shows the level of PrP-res relative to its level at time 0. The means and SD of four independent experiments are depicted.

In agreement with previous reports (Marijanovic *et al.*, 2009; Pimpinelli *et al.*, 2005; Taraboulos *et al.*, 1990; Veith *et al.*, 2009), we confirmed the widespread intracellular distribution of PrP^{Sc} throughout endocytic compartments in prion-infected cells (Fig. 3). PrP^{Sc} was not only present in early and late endosomes/lysosomes but also in cellular compartments at the peri-nuclear regions, at least some of which are thought to be the ERC, through which exogenously derived Tfn, StxB and CtxB are transported during their intracellular trafficking (Fig. 4). In this study, we observed the extensive co-localization of PrP^{Sc} with flotillin-1 in ScN2a-3-22L cells (Fig. 3). This result is inconsistent with the report by Pimpinelli *et al.* (2005), in which PrP^{Sc} in the Chandler strain-infected N2a cells was not co-localized well with flotillin-1. It remains to be elucidated how differences in prion strains and cell types influence the intracellular distribution of PrP^{Sc}.

Recent immunofluorescent and electron microscopy studies have also proposed the presence of PrP^{Sc} at the ERC (Godsave *et al.*, 2008; Marijanovic *et al.*, 2009). The ERC is a membranous tubular compartment in the vicinity of the nucleus and is defined by the presence of Rab11a and/or Tfn-bound Tfn receptor (Grant & Donaldson, 2009; Murphy *et al.*, 2005). Some internalized plasma membrane proteins such as Tfn receptor, the LDL receptor and GPI-anchored proteins including PrP^{C} are transported from the early endosomes to the ERC and are then sorted to their target sites including the plasma membrane (Magalhães *et al.*, 2002; Mayor & Riezman 2004; Morris *et al.*, 2006;

Prado *et al.*, 2004). Many proteins that cycle between the intracellular compartments and the cell surface are known to accumulate in the ERC (Maxfield & McGraw, 2004). Thus, the presence of PrP^{Sc} at the ERC raised the possibility that PrP^{Sc} in prion-infected cells is intracellularly transported with the membrane trafficking machinery that is associated with endocytic recycling. Although time-lapse imaging of trafficking PrP^{Sc} in cells persistently infected with prions is technically impossible at the moment, the kinetic analysis of PrP^{Sc} distribution in the cells shown in this study provided an interesting insight into the intracellular trafficking of PrP^{Sc} (Fig. 6). PrP^{Sc} granules at the peripheral regions including those at the plasma membrane appeared to increase during incubation at 20 °C, whereas peri-nuclear PrP^{Sc} granules gradually decreased under this condition. Conversely, peripheral PrP^{Sc} granules appeared to decrease as PrP^{Sc} granules accumulated at the peri-nuclear regions once the cells were transferred to 37 °C. This drastic alteration in the distribution of PrP^{Sc} during sequential incubation at 20 and 37 °C suggests that PrP^{Sc} is dynamically transported through compartments that exist at the peri-nuclear regions, at least some of which are thought to be the ERC, by the membrane trafficking machinery of the cell. Combined with the fact that PrP^{Sc} is present at the ERC as described above, it is conceivable that at least some of the PrP^{Sc} cycles between peri-nuclear and peripheral regions including the plasma membrane through the ERC, via the endocytic recycling pathway.

Marijanovic *et al.* (2009) reported that impairment of the transport from early endosomes to the ERC by overexpression of Rab22a reduced the level of PrP^{Sc}, but that impairment of transport from the ERC to the plasma membrane using a dominant-negative mutant of Rab11a increased the level of PrP^{Sc} in GT1 cells infected with prions. These findings suggest that the ERC is possibly one of the sites where PrP^{Sc} formation takes place. Although multiple trafficking pathways may be involved in the intracellular transport of PrP^{Sc} as suggested by the widespread distribution of PrP^{Sc} in prion-infected cells, cycling of PrP^{Sc} between the peri-nuclear and peripheral regions including the plasma membrane through the ERC, rather than accumulation of PrP^{Sc} at specific compartments, may provide a significant advantage for the generation of PrP^{Sc}. For instance, such cycling may provide increased opportunities for PrP^{Sc} to enter a site for conversion, which could then act as a seed for the conversion of PrP^{C} into PrP^{Sc}.

There are a few studies which report that PrP^{Sc} was detected in late endosomes or early endosomes/ERC in the brains of prion-infected animals (Arnold *et al.*, 1995; Godsave *et al.*, 2008). However, intracellular localization of PrP^{Sc} in brains of prion-infected animals is largely unknown. We have confirmed that mAb 132 is also applicable to the PrP^{Sc}-specific detection in brain section of prion-infected animals, and now experiments are under way to extensively analyse the cellular compartments where prions present in the brain of mice infected with prions.

METHODS

Antibodies, reagents and chemicals. Mouse mAbs, 31C6, 44B1, 149 and 132 were used for the detection of PrP. mAbs 31C6, 149 and 132 recognize linear epitopes consisting of mouse PrP aa 143–149, 147–151 and 119–127, respectively, whereas mAb 44B1 recognizes a discontinuous epitope consisting of aa 155–231 (Kim *et al.*, 2004b). Following antibodies were used for IFA: anti-Lamp1 rat mAb (1D4B; Beckman Coulter); rabbit polyclonal antibodies: anti-Tgn38 (ab16059; Abcam), anti-giantin (PRB-114C; Covance), anti-flotillin-1 (F1180; Sigma), anti-Rab5 (#2143), anti-Rab7 (#2094) and anti-Rab11a (#3539) (all three from Cell Signaling Technology), anti-Rab4a (10347-1-AP) and anti-Rab9 (11420-1-AP) (Proteintech Group Inc.). An affinity purified anti-StxB rabbit polyclonal antibody was prepared from polyclonal antiserum raised by immunizing a rabbit with purified StxB1-H and StxB2-H (Shimizu *et al.*, 2007). Alexa-Fluor-488- or 546-conjugated goat $F(ab')_2$ fragment anti-mouse IgG, Alexa-Fluor-555-conjugated goat $F(ab')_2$ fragment anti-rabbit IgG and Alexa-Fluor-555-conjugated goat IgG anti-rat IgG (Invitrogen) were used as secondary antibodies for IFA.

Cell culture. Subclones of mouse neuroblastoma cell line Neuro2a, N2a-3 (Uryu *et al.*, 2007), and of the hypothalamic neuronal cell line GT1, GT1-7 (Schätzl *et al.*, 1997), were used. As prion-infected cells, ScN2a-3-Ch (Uryu *et al.*, 2007), ScN2a-3-22L (Nakamitsu *et al.*, 2010) and ScGT1-7-22L were used. These prion-infected cells maintain PrP^{Sc} without significant loss of PrP^{Sc} more than 50 passages. However, we usually used these cells of passage history between 10 and 30 times. N2a-derived cells were passaged at a 1 : 10 dilution ratio every 3–4 days and were cultured in Dulbecco's modified Eagle's medium (DMEM; ICN Biomedicals) containing 10 % FBS (Gibco), MEM non-essential amino acids (NEAA; Gibco), penicillin (100 U ml^{-1}) and streptomycin (100 μg ml^{-1}) (Gibco) at 37 °C in 5 % CO_2 atmosphere. The GT1-7 cells were passaged at a 1 : 5 dilution ratio every 7 days and were cultured in DMEM containing 5 % FBS, 5 % horse serum (Gibco) and penicillin/streptomycin.

IFA. Cells grown on a Lab-Tek II CC2 eight-well chamber slide (Nunc) were fixed with pre-warmed PBS containing 4 % paraformaldehyde and 4 % sucrose at 37 °C or at room temperature (RT) for 10 min. After removal of the fixation solution, the remaining paraformaldehyde was neutralized with 0.1 M glycine in PBS for 10 min and then the cells were permeabilized with 0.1 % saponin in PBS for 10 min. For the detection of PrP^{Sc}, cells were pre-treated with 5 M GdnSCN for 10 min. The cells were then washed once with PBS and blocked with 5 % FBS in PBS at RT for 30 min. After blocking, the cells were incubated with primary antibodies in PBS containing 0.5 % FBS at 4 °C overnight. Anti-PrP mAbs were used at a concentration of 1 μg ml^{-1}. A mAb P2-284 (1 μg ml^{-1}) against feline panleukopenia virus was used as a negative-control antibody (Horiuchi *et al.*, 1997). After washing five times with PBS, the cells were incubated with Alexa-Fluor-conjugated secondary antibodies (1 : 1000) at RT for 90 min. For counterstaining of cell nuclei, cells were incubated for 30 min with 5 μg DAPI ml^{-1} (Invitrogen) in PBS at RT. The samples were then mounted with ProLong Gold antifade reagent (Invitrogen) and covered with coverslips. The samples were examined using a Nikon C1 laser confocal fluorescence microscope (Nikon) or with a Zeiss laser scanning microscope LSM 700 (Zeiss).

Tfn, CtxB and StxB uptake experiments. For analysis of Tfn uptake, cells grown on Lab-Tek chamber slide were washed twice with Opti-MEM (Gibco) and incubated with 10 μg Alexa-Fluor-555-conjugated Tfn (Invitrogen) ml^{-1} in Opti-MEM at 37 °C for 15 min. The cells were then washed three times with pre-warmed PBS and incubated at 37 °C for up to 30 min. For analysis of the uptake of CtxB, cells grown on a Lab-Tek chamber slide were washed with

Opti-MEM and incubated with 2 μg Alexa-Fluor-488-conjugated CtxB (Invitrogen) ml^{-1} in Opti-MEM at 4 °C for 30 min. For analysis of StxB uptake (Shimizu *et al.*, 2007), cells grown on a Lab-Tek chamber slide were washed with Opti-MEM and incubated with 2 μg StxB ml^{-1} in Opti-MEM at 4 °C for 60 min. The medium was then replaced with pre-warmed fresh DMEM and the cells were incubated at 37 °C for up to 60 min.

Immunoblotting of PrP-res. ScN2a-3-22L cells on 60 mm dishes were washed once with PBS, collected using a cell scraper and the cell number was counted. The collected cells were lysed with lysis buffer (Uryu *et al.*, 2007) at 4 °C for 20 min and cell debris was removed by centrifugation at 2000 ***g***. The protein concentration of the lysates was measured using the DC protein assay kit (Bio-Rad) and was adjusted to 1 mg ml^{-1}. The lysates (300 μl) were digested with 20 μg PK ml^{-1} at 37 °C for 20 min. The proteolysis was terminated by the addition of Pefabloc (Roche) to 1 mM. The PK-treated lysates were incubated with 0.3 % phosphotungstic acid at RT for 20 min and then centrifuged at 20 000 ***g*** for 20 min to precipitate PK-resistant PrP (PrP-res). The pellet was dissolved in SDS sample buffer and boiled for 5 min. A sample volume equivalent to 4×10^5 cells was loaded onto a NuPAGE 12 % Bistris gel (Invitrogen). SDS-PAGE was carried out according to the manufacturer's instructions (Invitrogen). Subsequent Western transfer and chemiluminescence were carried out as described previously (Shindoh *et al.*, 2009).

ACKNOWLEDGEMENTS

T. Y. is supported by a Grant-in-Aid for JSPS Fellows (grant no. 22.4181). This work was supported by a Grant-in-Aid for Science Research (A) (grant no. 23248050) and for challenging Exploratory Research (grant no. 23658233), a grant from the global COE Program (F-001), and the Program of Founding Research Centers for Emerging and Reemerging Infectious Diseases, from the Ministry of Education, Culture, Sports, Science, and Technology, Japan. This work was also supported by grants for TSE research (H23-Shokuhin-Ippan-005) and Research on Measures for Intractable Diseases from the Ministry of Health, Labour and Welfare of Japan. This work was also partly supported by a Grant-in-Aid from the BSE Control Project of the Ministry of Agriculture, Forestry and Fisheries of Japan. We thank Zensho Co., Ltd, for the BSL3 facility.

REFERENCES

Arnold, J. E., Tipler, C., Laszlo, L., Hope, J., Landon, M. & Mayer, R. J. (1995). The abnormal isoform of the prion protein accumulates in late-endosome-like organelles in scrapie-infected mouse brain. *J Pathol* **176**, 403–411.

Browman, D. T., Hoegg, M. B. & Robbins, S. M. (2007). The SPFH domain-containing proteins: more than lipid raft markers. *Trends Cell Biol* **17**, 394–402.

Callahan, M. A., Xiong, L. & Caughey, B. (2001). Reversibility of scrapie-associated prion protein aggregation. *J Biol Chem* **276**, 28022–28028.

Campana, V., Sarnataro, D. & Zurzolo, C. (2005). The highways and byways of prion protein trafficking. *Trends Cell Biol* **15**, 102–111.

Dron, M., Dandoy-Dron, F., Farooq Salamat, M. K. & Laude, H. (2009). Proteasome inhibitors promote the sequestration of PrP^{Sc} into aggresomes within the cytosol of prion-infected CAD neuronal cells. *J Gen Virol* **90**, 2050–2060.

Fournier, J. G., Escaig-Haye, F. & Grigoriev, V. (2000). Ultrastructural localization of prion proteins: physiological and pathological implications. *Microsc Res Tech* **50**, 76–88.

Gasset, M., Baldwin, M. A., Lloyd, D. H., Gabriel, J. M., Holtzman, D. M., Cohen, F., Fletterick, R. & Prusiner, S. B. (1992). Predicted alpha-helical regions of the prion protein when synthesized as peptides form amyloid. *Proc Natl Acad Sci U S A* **89**, 10940–10944.

Glebov, O. O., Bright, N. A. & Nichols, B. J. (2006). Flotillin-1 defines a clathrin-independent endocytic pathway in mammalian cells. *Nat Cell Biol* **8**, 46–54.

Godsave, S. F., Wille, H., Kujala, P., Latawiec, D., DeArmond, S. J., Serban, A., Prusiner, S. B. & Peters, P. J. (2008). Cryo-immunogold electron microscopy for prions: toward identification of a conversion site. *J Neurosci* **28**, 12489–12499.

Grant, B. D. & Donaldson, J. G. (2009). Pathways and mechanisms of endocytic recycling. *Nat Rev Mol Cell Biol* **10**, 597–608.

Horiuchi, M., Mochizuki, M., Ishiguro, N., Nagasawa, H. & Shinagawa, M. (1997). Epitope mapping of a monoclonal antibody specific to feline panleukopenia virus and mink enteritis virus. *J Vet Med Sci* **59**, 133–136.

Horiuchi, M., Karino, A., Furuoka, H., Ishiguro, N., Kimura, K. & Shinagawa, M. (2009). Generation of monoclonal antibody that distinguishes PrP^{Sc} from PrP^{C} and neutralizes prion infectivity. *Virology* **394**, 200–207.

Jeffrey, M., Goodsir, C. M., Bruce, M. E., McBride, P. A., Scott, J. R. & Halliday, W. G. (1992). Infection specific prion protein (PrP) accumulates on neuronal plasmalemma in scrapie infected mice. *Neurosci Lett* **147**, 106–109.

Kim, C.-L., Karino, A., Ishiguro, N., Shinagawa, M., Sato, M. & Horiuchi, M. (2004a). Cell-surface retention of PrP^{C} by anti-PrP antibody prevents protease-resistant PrP formation. *J Gen Virol* **85**, 3473–3482.

Kim, C.-L., Umetani, A., Matsui, T., Ishiguro, N., Shinagawa, M. & Horiuchi, M. (2004b). Antigenic characterization of an abnormal isoform of prion protein using a new diverse panel of monoclonal antibodies. *Virology* **320**, 40–51.

Kocisko, D. A., Lansbury, P. T., Jr & Caughey, B. (1996). Partial unfolding and refolding of scrapie-associated prion protein: evidence for a critical 16-kDa C-terminal domain. *Biochemistry* **35**, 13434–13442.

Korth, C., Stierli, B., Streit, P., Moser, M., Schaller, O., Fischer, R., Schulz-Schaeffer, W., Kretzschmar, H., Raeber, A. & other authors (1997). Prion (PrP^{Sc})-specific epitope defined by a monoclonal antibody. *Nature* **390**, 74–77.

Kristiansen, M., Messenger, M. J., Klöhn, P. C., Brandner, S., Wadsworth, J. D., Collinge, J. & Tabrizi, S. J. (2005). Disease-related prion protein forms aggresomes in neuronal cells leading to caspase activation and apoptosis. *J Biol Chem* **280**, 38851–38861.

Lieu, Z. Z. & Gleeson, P. A. (2010). Identification of different itineraries and retromer components for endosome-to-Golgi transport of TGN38 and Shiga toxin. *Eur J Cell Biol* **89**, 379–393.

Lin, A. E. & Guttman, J. A. (2010). Hijacking the endocytic machinery by microbial pathogens. *Protoplasma* **244**, 75–90.

Magalhães, A. C., Silva, J. A., Lee, K. S., Martins, V. R., Prado, V. F., Ferguson, S. S., Gomez, M. V., Brentani, R. R. & Prado, M. A. (2002). Endocytic intermediates involved with the intracellular trafficking of a fluorescent cellular prion protein. *J Biol Chem* **277**, 33311–33318.

Mallard, F., Antony, C., Tenza, D., Salamero, J., Goud, B. & Johannes, L. (1998). Direct pathway from early/recycling endosomes to the Golgi apparatus revealed through the study of shiga toxin B-fragment transport. *J Cell Biol* **143**, 973–990.

Marijanovic, Z., Caputo, A., Campana, V. & Zurzolo, C. (2009). Identification of an intracellular site of prion conversion. *PLoS Pathog* **5**, e1000426.

Maxfield, F. R. & McGraw, T. E. (2004). Endocytic recycling. *Nat Rev Mol Cell Biol* **5**, 121–132.

Mayor, S. & Riezman, H. (2004). Sorting GPI-anchored proteins. *Nat Rev Mol Cell Biol* **5**, 110–120.

McKinley, M. P., Taraboulos, A., Kenaga, L., Serban, D., Stieber, A., DeArmond, S. J., Prusiner, S. B. & Gonatas, N. (1991). Ultrastructural localization of scrapie prion proteins in cytoplasmic vesicles of infected cultured cells. *Lab Invest* **65**, 622–630.

Morris, R. J., Parkyn, C. J. & Jen, A. (2006). Traffic of prion protein between different compartments on the neuronal surface, and the propagation of prion disease. *FEBS Lett* **580**, 5565–5571.

Murphy, A. S., Bandyopadhyay, A., Holstein, S. E. & Peer, W. A. (2005). Endocytotic cycling of PM proteins. *Annu Rev Plant Biol* **56**, 221–251.

Nakamitsu, S., Kurokawa, A., Yamasaki, T., Uryu, M., Hasebe, R. & Horiuchi, M. (2010). Cell density-dependent increase in the level of protease-resistant prion protein in prion-infected Neuro2a mouse neuroblastoma cells. *J Gen Virol* **91**, 563–569.

Nichols, B. J., Kenworthy, A. K., Polishchuk, R. S., Lodge, R., Roberts, T. H., Hirschberg, K., Phair, R. D. & Lippincott-Schwartz, J. (2001). Rapid cycling of lipid raft markers between the cell surface and Golgi complex. *J Cell Biol* **153**, 529–542.

Paramithiotis, E., Pinard, M., Lawton, T., LaBoissiere, S., Leathers, V. L., Zou, W. Q., Estey, L. A., Lamontagne, J., Lehto, M. T. & other authors (2003). A prion protein epitope selective for the pathologically misfolded conformation. *Nat Med* **9**, 893–899.

Pimpinelli, F., Lehmann, S. & Maridonneau-Parini, I. (2005). The scrapie prion protein is present in flotillin-1-positive vesicles in central- but not peripheral-derived neuronal cell lines. *Eur J Neurosci* **21**, 2063–2072.

Prado, M. A., Alves-Silva, J., Magalhães, A. C., Prado, V. F., Linden, R., Martins, V. R. & Brentani, R. R. (2004). PrP^C on the road: trafficking of the cellular prion protein. *J Neurochem* **88**, 769–781.

Prusiner, S. B. (1998). Prions. *Proc Natl Acad Sci U S A* **95**, 13363–13383.

Ren, M., Xu, G., Zeng, J., De Lemos-Chiarandini, C., Adesnik, M. & Sabatini, D. D. (1998). Hydrolysis of GTP on rab11 is required for the direct delivery of transferrin from the pericentriolar recycling compartment to the cell surface but not from sorting endosomes. *Proc Natl Acad Sci U S A* **95**, 6187–6192.

Schätzl, H. M., Laszlo, L., Holtzman, D. M., Tatzelt, J., DeArmond, S. J., Weiner, R. I., Mobley, W. C. & Prusiner, S. B. (1997). A hypothalamic neuronal cell line persistently infected with scrapie prions exhibits apoptosis. *J Virol* **71**, 8821–8831.

Shimizu, T., Kawakami, S., Sato, T., Sasaki, T., Higashide, M., Hamabata, T., Ohta, T. & Noda, M. (2007). The serine 31 residue of the B subunit of Shiga toxin 2 is essential for secretion in enterohemorrhagic *Escherichia coli*. *Infect Immun* **75**, 2189–2200.

Shindoh, R., Kim, C.-L., Song, C.-H., Hasebe, R. & Horiuchi, M. (2009). The region approximately between amino acids 81 and 137 of proteinase K-resistant PrP^{Sc} is critical for the infectivity of the Chandler prion strain. *J Virol* **83**, 3852–3860.

Silveira, J. R., Raymond, G. J., Hughson, A. G., Race, R. E., Sim, V. L., Hayes, S. F. & Caughey, B. (2005). The most infectious prion protein particles. *Nature* **437**, 257–261.

Sipe, D. M., Jesurum, A. & Murphy, R. F. (1991). Absence of Na^+, K^+-ATPase regulation of endosomal acidification in K562 erythroleukemia cells. Analysis via inhibition of transferrin recycling by low temperatures. *J Biol Chem* **266**, 3469–3474.

Stenmark, H. (2009). Rab GTPases as coordinators of vesicle traffic. *Nat Rev Mol Cell Biol* **10**, 513–525.

Taraboulos, A., Serban, D. & Prusiner, S. B. (1990). Scrapie prion proteins accumulate in the cytoplasm of persistently infected cultured cells. *J Cell Biol* **110**, 2117–2132.

Uryu, M., Karino, A., Kamihara, Y. & Horiuchi, M. (2007). Characterization of prion susceptibility in Neuro2a mouse neuroblastoma cell subclones. *Microbiol Immunol* **51**, 661–669.

Veith, N. M., Plattner, H., Stuermer, C. A., Schulz-Schaeffer, W. J. & Bürkle, A. (2009). Immunolocalisation of PrP^{Sc} in scrapie-infected N2a mouse neuroblastoma cells by light and electron microscopy. *Eur J Cell Biol* **88**, 45–63.

JOURNAL OF VIROLOGY, Nov. 2011, p. 11069–11078 Vol. 85, No. 21
0022-538X/11/$12.00 doi:10.1128/JVI.05318-11

Identification of Chemoattractive Factors Involved in the Migration of Bone Marrow-Derived Mesenchymal Stem Cells to Brain Lesions Caused by Prions[▽]

Chang-Hyun Song,[1]† Osamu Honmou,[2] Hidefumi Furuoka,[3] and Motohiro Horiuchi[1]*

Laboratory of Veterinary Hygiene, Graduate School of Veterinary Medicine, Hokkaido University, Kita 18, Nishi 9, Kita-ku, Sapporo 060-0818, Japan[1]; Departments of Neural Repair and Therapeutics, Sapporo Medical University, South-1st, West-16th, Chuo-ku, Sapporo 060-8543, Japan[2]; and Department of Pathobiological Science, Obihiro University of Agriculture and Veterinary Medicine, Inada-cho, Obihiro 080-8555, Japan[3]

Received 7 June 2011/Accepted 27 July 2011

Bone marrow-derived mesenchymal stem cells (MSCs) have been reported to migrate to brain lesions of neurodegenerative diseases; however, the precise mechanisms by which MSCs migrate remain to be elucidated. In this study, we carried out an *in vitro* migration assay to investigate the chemoattractive factors for MSCs in the brains of prion-infected mice. The migration of immortalized human MSCs (hMSCs) was reduced by their pretreatment with antibodies against the chemokine receptors, CCR3, CCR5, CXCR3, and CXCR4 and by pretreatment of brain extracts of prion-infected mice with antibodies against the corresponding ligands, suggesting the involvement of these receptors, and their ligands in the migration of hMSCs. In agreement with the results of an *in vitro* migration assay, hMSCs in the corpus callosum, which are considered to be migrating from the transplanted area toward brain lesions of prion-infected mice, expressed CCR3, CCR5, CXCR3, and CXCR4. The combined *in vitro* and *in vivo* analyses suggest that CCR3, CCR5, CXCR3, and CXCR4, and their corresponding ligands are involved in the migration of hMSCs to the brain lesions caused by prion propagation. In addition, hMSCs that had migrated to the right hippocampus of prion-infected mice expressed CCR1, CX3CR1, and CXCR4, implying the involvement of these chemokine receptors in hMSC functions after chemotactic migration. Further elucidation of the mechanisms that underlie the migration of MSCs may provide useful information regarding application of MSCs to the treatment of prion diseases.

Prion diseases are fatal neurodegenerative disorders in humans and animals that are characterized by the accumulation of a disease-specific isoform of the prion protein (PrP^{Sc}), astrocytosis, microglial activation, spongiosis, and neuronal cell death in the central nervous system (CNS). Although the etiology of the diseases is not clear, conversion of the normal prion protein to PrP^{Sc} plays a key role in the neuropathological changes (44). Therefore, compounds that inhibit PrP^{Sc} formation are considered as therapeutic candidates of the diseases, and many compounds have been reported to inhibit PrP^{Sc} formation in cell cultures and cell-free systems (reviewed in reference 56). However, only a few of these inhibitors, such as amphotericin B and its derivative (13), pentosan polysulfate (14), porphyrin derivatives (27), certain amyloidophilic compounds (25), and FK506 (37) have been reported to prolong the survival of prion-infected mice even when administered in the middle-late stage of infection but still before clinical onset. We recently reported that intraventricular infusion of anti-PrP antibodies (50) slowed down the progression of the disease even when initiated just after clinical onset. However, in addition to inhibition of PrP^{Sc} formation, the protection of neurons or restoration of degenerated neurons is thought to be important for functional recovery.

Bone marrow-derived mesenchymal stem cells (MSCs) differentiate into cells of mesodermal origin such as adipocytes, osteoblasts, and endothelial and muscle cells (41, 43). In addition, MSCs are known to transdifferentiate into neuronal and glial cells. MSCs have been shown to migrate to damaged neuronal tissues and to alleviate the deficits in experimental animal models of cerebral ischemia (10), spinal cord injury (20), Parkinson's disease (19, 33), and amyotrophic lateral sclerosis (59). MSCs also secrete various neurotrophic factors that may protect neuronal tissues from degradations, as well as stimulate the activity of endogenous neural stem cells (38). Therefore, despite their mesodermal origin, MSCs are considered to be a candidate for cell-mediated therapy for neurodegenerative diseases. One of the characteristics of MSCs is their migration to brain lesions caused by neurodegenerative diseases, including prion diseases (10, 19, 39, 51). This feature may be of further use for cell-mediated therapy of neurodegenerative diseases, particularly for prion diseases, Multiple sclerosis and Alzheimer's disease, which have diffuse pathological lesions.

Since many cytokines, chemokines, and adhesion molecules are involved in the homing of immune cells (9, 36, 53), evidence that a variety of chemokines and growth factors, as well as their cognate receptors, have a pivotal role in the migration of MSCs has been accumulated. These factors include CXCL12 and its receptor CXCR4 (30, 40; reviewed in reference 52), CCL2 (15, 62, 66), CCL3 (62), interleukin-8 (48, 62),

* Corresponding author. Mailing address: Laboratory of Veterinary Hygiene, Graduate School of Veterinary Medicine, Hokkaido University, Kita 18, Nishi 9, Kita-ku, Sapporo 060-0818, Japan. Phone and fax: 81-11-706-5293. E-mail: horiuchi@vetmed.hokudai.ac.jp.

† Present address: Department of Neurology, Emory University School of Medicine, Woodruff Memorial Building, 101 Woodruff Circle, Atlanta, GA 30322.

▽ Published ahead of print on 3 August 2011.

hepatocyte growth factor (16), platelet-derived growth factor AB (PDGF-AB), insulin-like growth factor 1 (IGF-1), CCL5 and CCL22 (42), and integrin β1 (23). Regarding the migration of MSCs to injury in the CNS, the involvement of CCL2 (61), CXCL12/CXCR4, and CX3CL1/CX3CR1 (24) has been reported. However, knowledge of the mechanism by which MSCs migrate to pathological lesions of neurodegenerative diseases is insufficient, and further efforts are required to elucidate this mechanism.

We recently reported that human MSCs (hMSCs) migrate to CNS lesions and prolong the survival of mice infected with prions (51). In the present study, we investigated factors that are involved in the migration of hMSCs to brain lesions of prion diseases.

MATERIALS AND METHODS

Cell culture. Human bone marrow-derived MSCs that were immortalized with the human telomerase catalytic subunit gene (26) and that stably expressed the LacZ gene (hMSCs [51]) were used. The hMSCs were cultured in Dulbecco modified Eagle medium (DMEM; Sigma Chemical Co., St. Louis, MO) containing 10% fetal bovine serum (FBS) in a humidified atmosphere under normoxic (21% O_2 and 5% CO_2) or hypoxic (2% O_2 and 5% CO_2) conditions at 37°C.

Mice and prion inoculation. All animal experiments were carried out according to protocols approved by the Institutional Committee for Animal Experiments. Four-week-old female ICR mice were purchased from CLEA Japan, Inc. (Japan), and the mice were acclimatized for a week prior to use. Brain homogenates (10% [wt/wt] in phosphate-buffered saline [PBS]) that were used for inoculation were prepared from brains of mice infected with the Chandler prion strain at the terminal stage of the disease and from age-matched uninfected mice. Mice were intracerebrally inoculated with 20 μl of 10% brain homogenates.

In vitro migration assay. To examine the migration of hMSCs *in vitro*, the brains of infected mice 120 days postinoculation (dpi) with the Chandler strain or of age-matched mock-infected mice were homogenized to 20% (wt/wt) in DMEM. The homogenates were centrifuged at 10,000 × *g* for 10 min at 4°C, and the resulting supernatants were passed through a 0.22-μm-pore-size filter. Aliquots of the brain extracts were stored at −80°C until use. Migration of hMSCs to the brain extracts was assessed using a QCM chemotaxis cell migration assay kit (Chemicon, Temecula, CA). The hMSCs that were starved for a day in serum-free medium were harvested, and 300 μl of cell suspension (5×10^4 cells) was added to the insert well. The lower chambers were supplied with serum-free DMEM containing 1% brain extract. At 24 h after incubation, hMSCs on the polycarbonate membrane (pore size, 8.0 μm) were stained with the cell stain solution provided in the kit. Nonmigratory cells that stayed on the upper side of the polycarbonate membrane were removed using a cotton swab. The migrated hMSCs, which had passed through the pores and clung to the underside of the membrane, were counted using the NIH Image J program. Three random high-magnification (×100) light microscopic images were captured using the Olympus BX-51 microscope and were used for cell counting.

To examine the involvement of receptors expressed on hMSCs in their migration, hMSCs were preincubated with antibodies against specific receptors for 30 min before adding the insert wells. To examine the involvement of chemokines and growth factors in migration, 1% brain homogenates were incubated with antibodies against specific chemokines and growth factors for 30 min at 4°C prior to adding them to the insert wells. Antibodies against various proteins were purchased as follows: PDGF-αβ receptor (PDGF-αβR, ab34074), CCR2 (ab1668), CCR4 (ab1669), CX3CR1 (ab7201), CXCR3 (clone 2Ar1), and CCL3 (ab10381) were from Abcam (Cambridge, MA); IGF-1 receptor (IGF-1R; clone 33255), CXCR4 (clone 12G5), IGF-1 (AF791), CCL2 (clone 123602), CCL4 (AF-451-NA), CCL5 (AF-478), CCL7 (AF-456-NA), CCL17 (AF-529), CCL24 (clone 106521), CX3CL1 (clone 126315), CXCL10 (AF-466-NA), CXCL12 (clone 79014), and CXCL13 (AF-470) were from R&D Systems (Minneapolis, MN); CCR1 (clone 141-2) and CCR3 (clone 444-11) were both from MRL; CCR5 (clone 45523.111) was from (Sigma Chemical Co.); and PDGF-AB (06-127) was from Millipore (Billerica, MA). All antibodies were used at a concentration of 10 μg/ml. Migration assays were performed as three independent experiments (each experiment was carried out in triplicate).

Transplantation of hMSCs. The hMSCs were transplanted into the thalamus as described previously (51). Briefly, after anesthesia, mouse scalps were incised. The mice were then placed onto a stereotaxic apparatus (Narishige, Japan), and burr holes were drilled to accommodate stereotaxic placement into the thalamus (caudal, 2.0 mm; lateral, 2.1 mm; depth, 3.2 mm [Bregma]). The hMSCs (10^5 cells in 2 μl of DMEM) were transplanted over a period of 15 min using a Hamilton syringe with a 31-gauge needle.

Flow cytometric analysis. The hMSCs were treated with 1 mM EDTA and dispersed in 0.5% FBS in PBS (FBS-PBS) by pipetting. The cells were then incubated with primary mouse antibodies against IGF-1R, CCR1, CCR3, CCR5, CXCR3, and CXCR4, primary goat antibodies against PDGF-αβR, CCR2, and CCR4, and a primary rabbit antibody against CX3CR1 (all at a 1:200 dilution) in 0.5% FBS-PBS for 30 min on ice. The primary antibodies were omitted for negative controls. The cells were washed three times with 0.5% FBS-PBS and incubated with anti-mouse Alexa Fluor 546, anti-goat Alexa Fluor 555, or anti-rabbit Alexa Fluor 555 (Molecular Probes, Eugene, OR) at a 1:1,000 dilution for 30 min on ice. After washing, the cells were stained with 5 μg/ml of propidium iodide (Molecular Probes) in PBS for 5 min and analyzed using an EPICS XL-ADC flow cytometer (Beckman Coulter, Miami, FL).

Quantitative reverse transcription-PCR (qRT-PCR). Total RNA was obtained from hMSCs or from mouse brains using TRIzol reagent (Invitrogen Life Technologies, Carlsbad, CA). First-strand cDNA was synthesized from 2.5 μg of the total RNA using a First-Strand synthesis kit (Amersham Biosciences, United Kingdom) according to the manufacturer's instructions. Quantitative PCR was carried out using a TaqMan assay. The amplification reaction mixtures contained template cDNA, 1× predesigned TaqMan gene expression assays, and 1× TaqMan universal PCR master mix (Applied Biosystems, Foster City, CA) in a final reaction volume of 20 μl. The following TaqMan gene expression assays were purchased from Applied Biosystems: human genes for PDGF-αβR (assay identification Hs00182163), CCR3 (Hs00266213), CCR4 (Hs99999919), CCR5 (Hs99999149), CX3CR1 (Hs00365842), CXCR3 (Hs01847760), and CXCR4 (Hs00607978) and mouse genes for CCL3 (Mm00441259), CCL4 (Mm00443111), CCL5 (Mm01302427), CCL7 (Mm00443113), CCL17 (Mm01244826), CX3CL1 (Mm00436454), CXCL10 (Mm00445235), and CXCL12 (Mm00445553). The human RNase P gene or the mouse glyceraldehyde-3-phosphate dehydrogenase (GAPDH) gene was amplified as an internal marker using human RNase P control reagents (catalog no. 4316844; Applied Biosystems) or TaqMan rodent GAPDH control reagents (catalog no. 4308313; Applied Biosystems). TaqMan assays were carried out using an ABI Prism 7900HT sequence detection system (Applied Biosystems). The amplification profiles were analyzed using a threshold cycle (C_T) relative quantification method and were normalized to the expression of the human RNase P control gene or the mouse GAPDH gene, which were used as human and mouse reference genes as described previously (58).

IFA. Immunofluorescence assay (IFA) was performed on hMSCs cultured in an 8-well chamber slide (Nalge Nunc, Naperville, IL) or on cryosections (5 μm thick) of mouse brains after transplantation of hMSCs. The cells or sections were fixed with cold methanol for 20 min at −20°C and treated with PBS containing 0.1% polyoxyethylene (20) and sorbitan monolaurate (Tween 20) (PBST) for 10 min. After blocking with 5% FBS in PBST for 30 min, the cells or sections were incubated for 1 h with primary antibodies for the receptors described above using a 1:500 dilution. After being washed with PBST, they were then incubated with a 1:2,000 dilution of anti-mouse Alexa Fluor 546, anti-goat Alexa Fluor 555, or anti-rabbit Alexa Fluor 555 for 1 h at room temperature. To investigate the colocalization of hMSCs with their receptors, the sections were incubated for 90 min with a mouse anti-β-Gal antibody (catalog no. Z3783; Promega, Madison, WI) conjugated with Alexa Fluor 488 (51). After being washed with PBST, samples were then mounted with Vectashield containing DAPI (4′,6′-diamidino-2-phenylindole; Vector Laboratories, Burlingame, CA). Samples were observed under a Nikon C1 laser confocal microscope.

RESULTS

Migration of hMSCs to the brain extracts. Hypoxic preconditioning of MSCs is reported to enhance their migratory activity (2, 22). To determine the effects of oxygen conditions on the migration of hMSCs to brain homogenates of mock- or prion-infected mice, hMSCs that were cultured under normoxic or hypoxic conditions were analyzed using an *in vitro* migration assay. The hMSCs that were precultured under hypoxic conditions migrated to brain extracts of prion-infected mice more efficiently than those precultured under normoxic conditions (Fig. 1A). Quantitative analysis revealed that twice

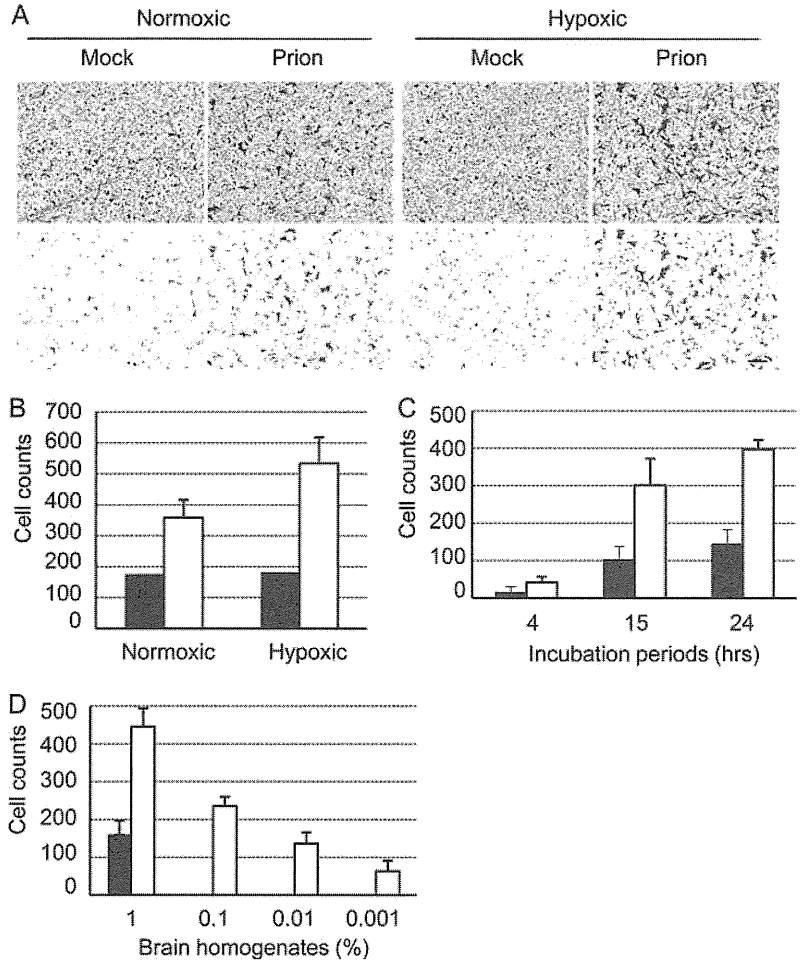

FIG. 1. Chemotactic migration of hMSCs to brain extracts of mock- or prion-infected mice. The migration of hMSCs to brain extracts of mock- or prion-infected mice that were prepared at 120 dpi was analyzed using a QCM 96-well cell migration assay kit. (A) hMSCs migrated to the underside of the membrane of the insert well. The hMSCs that were precultured under normoxic or hypoxic conditions (Normoxic or Hypoxic) were added to the insert well, and the lower chambers were supplied with serum-free DMEM containing 1% brain extracts of mock- or prion-infected mice (Mock or Prion). At 24 h after incubation, hMSCs that had passed through the pores of the membrane and clung to its underside were stained (upper panel). Stained cells with a size of >200 μm^2 were selected (lower panel) and counted using the NIH ImageJ program. Bar, 100 μm. (B) Quantification of migrated hMSCs. The migration of hMSCs, assayed as described in panel A, was quantified. Three random areas (3.84×10^5 μm^2/area) of the underside of the membrane were photographed, and the number of hMSCs was counted. The graphs show cell counts per 3.84×10^5 μm^2 (means and standard deviations [SDs] are shown; $n = 3$). Black and white bars indicate the numbers of hMSCs that migrated to 1% brain extracts of mock- and prion-infected mice, respectively. (C) Time-dependent increase in hMSC migration. The migration assay was performed for 4, 15, and 24 h. (D) Dose dependency of hMSC migration. The migration of hMSCs to various doses (0.001, 0.01, 0.1, and 1%) of the brain extracts was analyzed. The graph shows cell counts per 3.84×10^5 μm^2 at the underside of the membrane (means and SDs, $n = 3$).

as many hMSCs migrated to the brain extracts of prion-infected mice than to those of mock-infected mice following normoxic preconditioning, while 2.7 times more hMSCs migrated to the brain extracts of prion-infected mice following hypoxic preconditioning (Fig. 1B). No differences were observed in the migration of hMSCs to the brain extracts of mock-infected mice between normoxic and hypoxic preconditioning. We therefore used hMSCs that were precultured under hypoxic conditions for all subsequent experiments to facilitate discrimination between subtle differences in cell migration. These hMSCs showed a time-dependent increase in migration for up to 24 h (Fig. 1C), and their migration increased in a brain extract concentration-dependent manner (Fig. 1D). Migration of hMSCs to 0.01 and 0.001% brain homogenates of prion-infected mice was observed, whereas only migration to 1% brain homogenates, but not to lower percentages of brain extracts of mock-infected mice was observed.

Chemotactic factors involved in the migration of hMSCs. The chemokine CXCL12 and its receptor, CXCR4, are known to be involved in the chemotactic migration of MSCs to brain lesions of neurodegenerative diseases (24, 63). However, since MSCs express a variety of receptors for growth factors, chemokines and cytokines that are associated with cell migration (8, 52), it was anticipated that other cytokines, chemokines and

TABLE 1. Growth factor and chemokine receptors and their corresponding ligands[a]

Receptor[b]	Corresponding ligand(s)
HGFR	HGF
IGF-1R	IGF-1
PDGF-αβR	PDGF-AB
CCR1	CCL3, CCL5, CCL7, CCL13
CCR2	CCL2, CCL7, CCL8, CCL13
CCR3	CCL5, CCL7, CCL8, CCL11, CCL24
CCR4	CCL17, CCL22
CCR5	CCL3, CCL4, CCL5, CCL8, CCL11
CX3CR1	CX3CL1
CXCR3	CXCL9, CXCL10, CXCL11
CXCR4	CXCL12
CXCR5	CXCL13

[a] The table was adapted from that of Spaeth et al. (52).
[b] HGFR, hepatocyte growth factor receptor; IGFR, insulin-like growth factor receptor; PDGF-αβR, platelet-derived growth factor-αβ receptor.

growth factors also play a role in the migration of MSCs. We therefore selected 10 receptors for chemokines and growth factors, and 13 of their ligands, as indicated in Table 1, and analyzed their involvement in hMSC migration using an *in vitro* migration assay (Fig. 2). These factors were chosen with reference to cell surface expression of those receptors on MSCs in previous studies (50) and to the pathway and networks of receptors and their ligands obtained using Ingenuity Pathway Analysis 5.0 (Ingenuity System, Inc., Redwood City, CA). The migration of hMSCs to the brain extracts of prion-infected mice was significantly decreased when hMSCs were pretreated with antibodies against CCR3, CCR4, CCR5, CXCR3, and CXCR4 compared to the migration of untreated hMSCs ($P < 0.05$, Dunnett's test) (Fig. 2A). When antibodies against the ligands of these receptors were tested (Table 1), the migration of hMSCs was significantly decreased by treatment of the brain extracts with antibodies against the ligands for CCR3 (CCL5, CCL7, and CCL24), CCR5 (CCL3, CCL4, and CCL5), CXCR3 (CXCL10), and CXCR4 (CXCL12) ($P < 0.05$) (Fig. 2B). Neither the antibody against CX3CR1, nor that against its corresponding ligand, CX3CL1, decreased the migration of hMSCs. In addition, the antibody against CCR4 decreased hMSC migration, whereas the antibody against its ligand, CCL17, did not. When the involvement of growth factors and their receptors in migration was analyzed, antibodies against the PDGF-αβR or the IGF-1R did not decrease migration, whereas antibodies against their respective ligands, PDGF-AB and IGF-1, did decrease migration. In addition, an antibody against CCR2 or its ligand CCL2 did not decrease migration, but an antibody against CCL7, another ligand for CCR2, did decrease migration. Taking into account the biological relationship between the receptors and ligands that were analyzed here, the migration assays suggested that at least CCR3, CCR5, CXCR3, and CXCR4, and their ligands were involved in the migration of hMSCs to the brain extracts of prion-infected mice.

Expression of chemokine and chemokine receptor genes. We next examined the expression of chemokine genes in the brains of prion-infected mice and that of chemokine receptor genes in hMSCs treated with the brain extracts of prion-infected mice. For the latter analysis, hMSCs were incubated with DMEM containing 1% brain extracts of prion- or mock-infected mice. At 24 h after incubation, total RNA was recovered, and gene expression was analyzed using qRT-PCR. The expression of CCR3, CCR4, CCR5, and CXCR4 genes was elevated 2- to 9-fold in hMSCs treated with the brain extracts of prion-infected mice compared to their expressions in hMSCs that were treated with the brain extracts of mock-infected mice (Fig. 3A). In contrast, the expression of PDGF-αβR, CX3CR1, and CXCR3 genes was not upregulated by stimulation of the hMSCs with brain extracts from prion-infected mice.

The expression of chemokine genes in the brains of prion-infected mice or of age-matched control mice was also analyzed at 120 dpi. The expression of CCL3, CCL4, CCL5, and CXCL10 genes was upregulated by 10-fold (CXCL10 and CCL5) to nearly 50-fold (CCL3 and CCL4) in the brains of prion-infected mice (Fig. 3B). In addition, the mRNA levels of CCL7 and CCL17 (a ligand for CCR4) were moderately increased (ca. 3- to 6-fold) in the brains of prion-infected mice. In contrast, the expression of the CX3CL1 and CXCL12 genes was not upregulated.

Expression of chemokine receptors on hMSCs. Flow cytometric analysis and IFA were carried out to confirm the expression of chemokine and growth factor receptors on hMSCs.

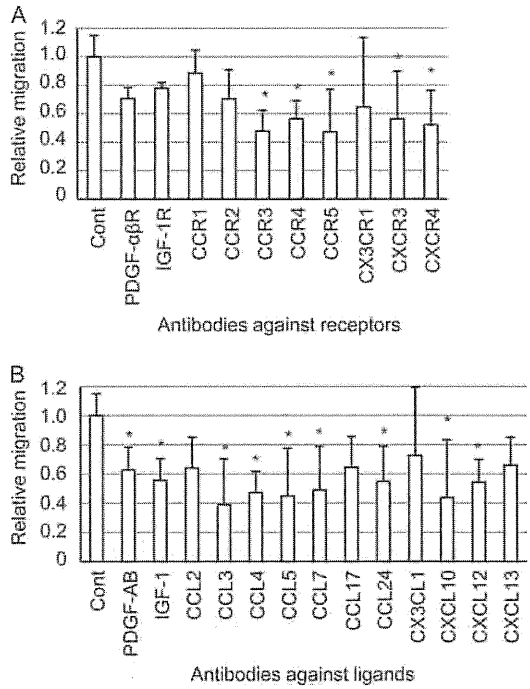

FIG. 2. Screening of chemotactic factors involved in the migration of hMSCs. The migration of hMSCs to 1% brain extracts of prion-infected mice was assessed after pretreatment of hMSCs with antibodies against receptors for chemokines or growth factors (A) or after pretreatment of brain extracts with antibodies against growth factors or chemokines (B). Migration assays, in which antibody pretreatments of hMSCs and brain extracts were omitted, were assigned as a control (Cont). The graphs show relative numbers of hMSCs that migrated to the brain extracts of prion-infected mice compared to numbers of hMSCs that migrated to brain extracts in control experiments. Means and SDs from three independent assays (each assay was carried out in triplicate) are shown. *, $P < 0.05$ (Dunnett's post hoc test).

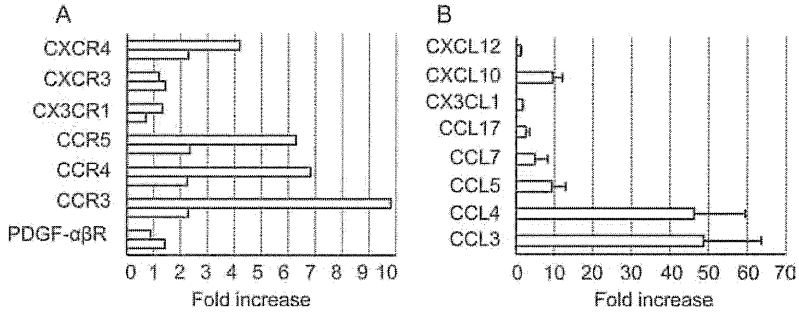

FIG. 3. Expression of chemokine receptor genes in hMSCs and chemokine genes in the brains of prion-infected mice. (A) Expression of chemokine and growth factor receptor genes in hMSCs stimulated with brain extracts of prion-infected mice. The hMSCs were incubated for a day in DMEM containing 1% brain extracts of prion-infected mice prepared at 120 dpi or of age-matched mock-infected mice. Expression of the mRNA of the indicated genes was then analyzed using qRT-PCR. The graph shows the fold increase in gene expression in hMSCs incubated with brain extracts of prion-infected mice compared to hMSCs incubated with brain extracts of mock-infected mice. The results of two independent experiments are shown. (B) Expression of chemokine genes in the brains of prion-infected mice. The graph shows the fold increases in gene expression in the brains of prion-infected mice at 120 dpi compared to the brains of age-matched mock-infected mice. Means and SDs (n = 3) of the fold increase are shown.

The hMSCs treated with brain extracts of mock-infected mice expressed PDGF-αβR, CCR3, CCR4, CXCR4, and CXCR3 on the cell surface. Of these receptors, expression of CCR3, CCR4, and CXCR4 was increased by stimulation with brain extracts of prion-infected mice, whereas no increase in expression of PDGF-αβR and CXCR3 was observed. Although it is difficult to distinguish signals on the plasma membrane from those in the cytoplasm using IFA, a similar tendency was observed in IFA; CCR3, CCR4, and CXCR4 fluorescent signals appeared to be more intense in cells treated with brain extracts of prion-infected mice than in cells treated with brain extracts of mock-infected mice. In contrast to the expression of these receptors, hMSCs expressed a trace level of CX3CR1, and CCR5 was not detectable on the cell surface. However, the expression of CCR5 was specifically induced in response to brain extracts of prion-infected mice (Fig. 4A). The prion-specific induction of CCR5 expression was also confirmed by IFA (Fig. 4B).

Differential expression of chemokine receptors on hMSCs after transplantation into the brains of prion-infected mice. It is known that MSCs transplanted into the left hippocampus or thalamus migrate to the contralateral (right) hippocampus through the corpus callosum (3, 19, 51). Therefore, we hypoth-

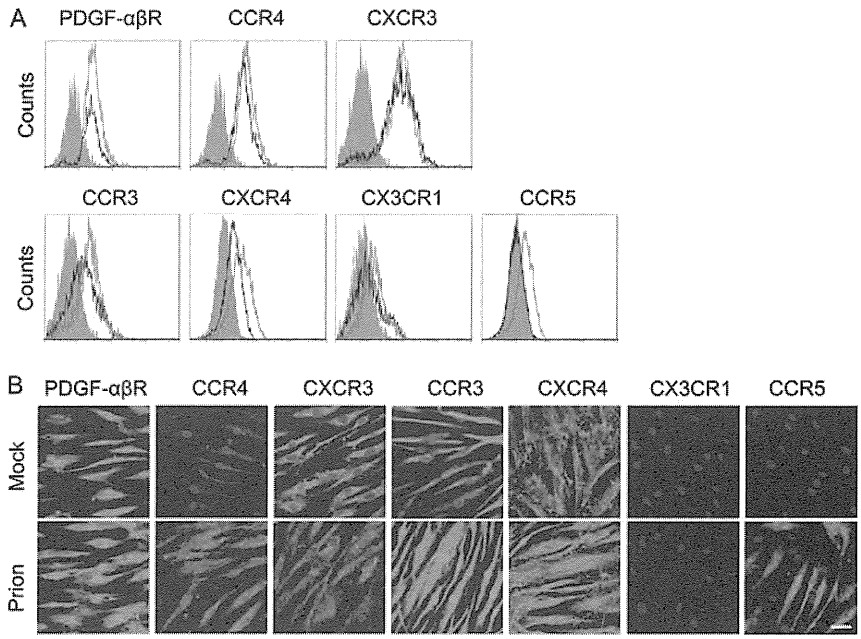

FIG. 4. Expression of chemokine receptors on hMSCs. (A) Flow cytometric analysis. The expression of chemokine receptors on the cell surface was examined after incubation of the cells with brain extracts of mock (black)- or prion (red)-infected mice prepared at 120 dpi. Gray histograms indicate the negative control (omitted primary antibodies). (B) IFA. The hMSCs that were incubated with brain extracts of mock- or prion-infected mice (Mock or Prion) for 24 h in 8-chamber slides were stained with antibodies against chemokine receptors (red) and were counterstained with DAPI (blue). Bar, 20 μm.

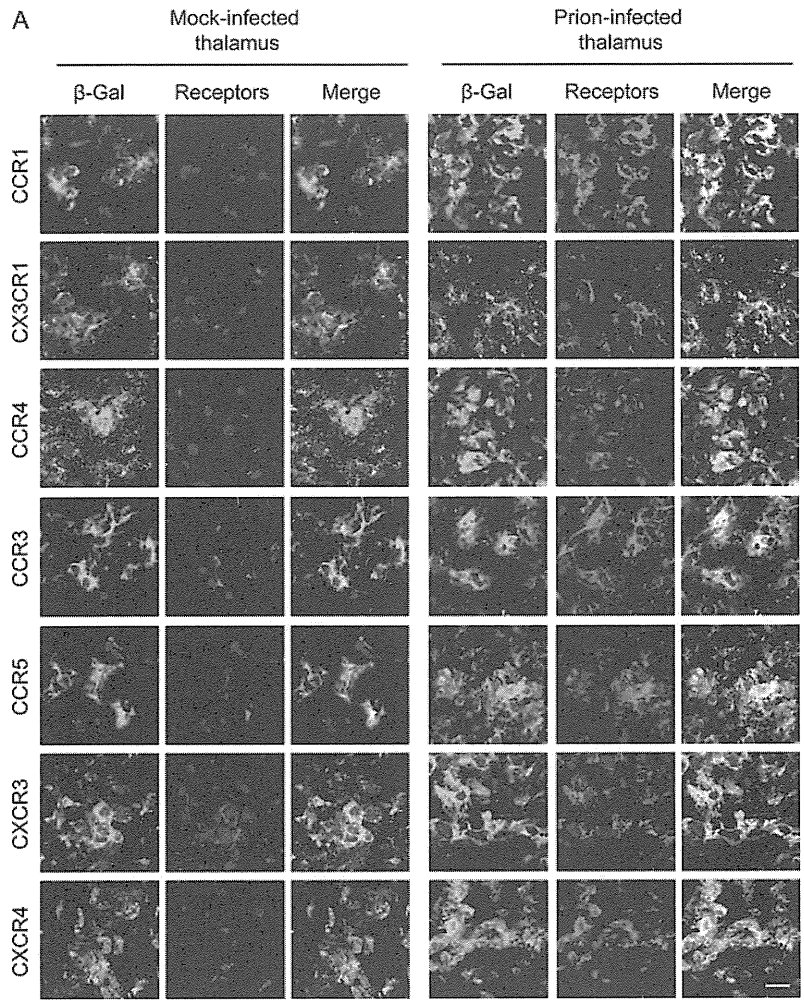

FIG. 5. Expression of chemokine receptors in hMSCs transplanted into the brains of mock- or prion-infected mice. The hMSCs (10^5 cells) were transplanted into the left thalamus of mock- or prion-infected mice at 120 dpi, and cryosections of mouse brains were prepared at 2 days or a week posttransplantation. Sections were double stained with anti-β-Gal antibodies conjugated with Alexa Fluor 488 (green) for staining of hMSCs and with antibodies against chemokine receptors (red). Nuclei were counterstained with DAPI (blue). (A) Expression of chemokine receptors in hMSCs at the transplanted area. Images of the left thalamus (transplanted side) of mock- and prion-infected mice were taken at 2 days posttransplantation. (B) Expression of chemokine receptors in hMSCs in the corpus callosum and the right hippocampus. Images of the corpus callosum and the right hippocampus (contralateral side) of prion-infected mice were taken at 2 days and 1 week posttransplantation, respectively. Bar, 20 μm.

esized that receptors expressed on hMSCs in the corpus callosum are possibly involved in the migration of hMSCs to neuropathological lesions. We therefore transplanted hMSCs into the left thalamus of prion- or mock-infected mice at 120 dpi and analyzed the expression of growth factor/chemokine receptors on hMSCs. Two days after transplantation of hMSCs into the left thalami of prion-infected mice, hMSCs in the transplanted region expressed CCR1, CCR3, CCR4, CCR5, CX3CR1, CXCR3, and CXCR4 (Fig. 5A), as well as PDGF-αβR, IGF-1R, and CCR2 (data not shown). However, the hMSCs that were transplanted into the mock-infected mice showed weak expression of these receptors except for CXCR3, suggesting that the expression of these chemokine receptors was increased by stimulation with factors produced in the brains of prion-infected mice. At 2 days posttransplantation, hMSCs in the corpus callosum of prion-infected mice still strongly expressed CCR3, CCR5, CXCR3, and CXCR4, but the expression of CCR1, CX3CR1, and CCR4 appeared to be lower than that on hMSCs in the transplanted area (Fig. 5B). The expression of chemokine receptors on hMSCs in the contralateral hippocampus also differed from that on hMSCs in the transplanted region and in the corpus callosum; hMSCs preferentially expressed only CCR1, CX3CR1, and CXCR4 in the contralateral hippocampus at 1 week posttransplantation (Fig. 5B). These data suggest that CCR1, CX3CR1, and CXCR4 may be associated with specific activities of hMSCs after their migration to the target lesions.

DISCUSSION

MSCs are known to migrate to neuropathological lesions of neurodegenerative diseases (8, 54). The migrated MSCs can

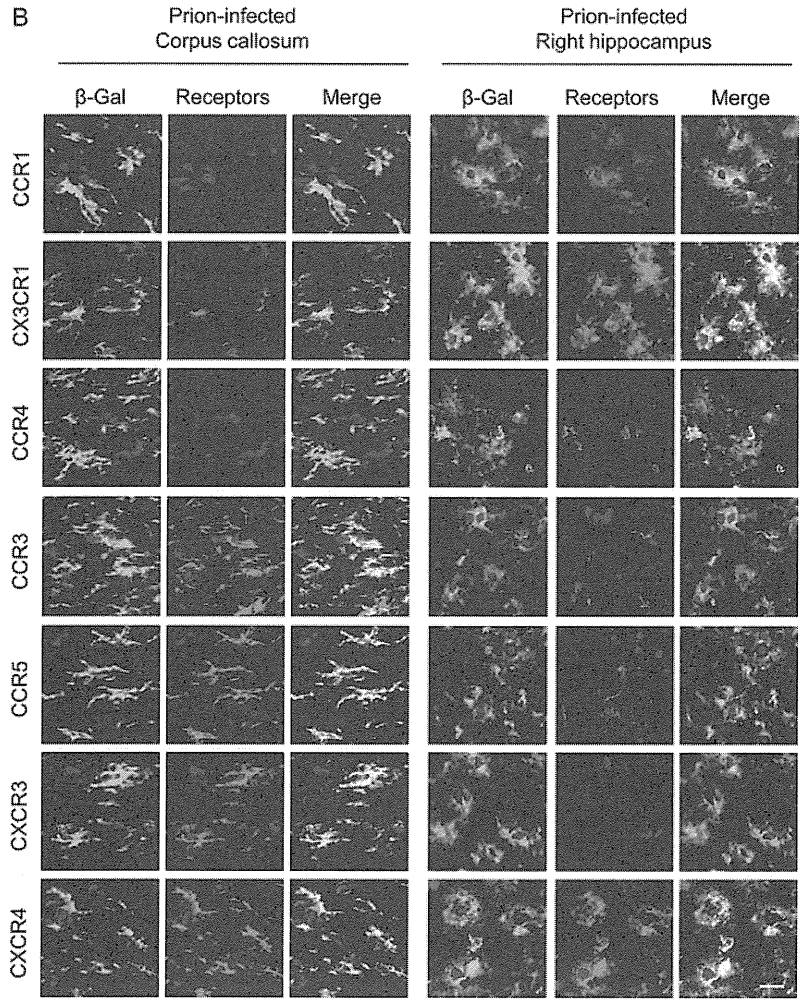

FIG. 5—*Continued.*

contribute to the functional recovery of damaged nervous tissues by secretion of various trophic factors (12), neuronal differentiation or cell fusion (1, 29), and stimulation of the proliferation and differentiation of endogenous neural stem cells (38). To date, transplantation of MSCs has been reported to ameliorate the symptoms not only of the experimental animal models of neurodegenerative diseases (10, 19, 20, 33, 59) but also of human patients with multiple system atrophy (32), amyotrophic lateral sclerosis (35), or stroke (4). The involvement of CXCL12 and its cognate receptor CXCR4 in MSC migration to injured tissues is well established (17) in spite of some exceptions (23). *In vitro* migration assays reported to date have identified growth factors and chemokines that are possibly involved in MSC migration (42, 49, 60, 61). However, the mechanisms of MSC migration are expected to differ with tissue microenvironments induced by diseases. Targeting of MSCs to neuropathological lesions is essential for functional recovery; therefore, an understanding of the mechanisms that underlie the migration of MSCs to lesions in the CNS could contribute to the development of MSC-mediated cell therapy by facilitating site-specific migration of MSCs. The involvement of CCL2, CXCL12/CXCR4, and CXCL1/CX3CR1 in the migration of MSCs to brain lesions has been reported (24, 62, 63). However, the mechanisms that underlie the migration of MSCs to neuropathological lesions are largely unknown.

We recently showed that hMSCs can migrate to neuropathological lesions induced by prion propagation (51). Since brain extracts of prion-infected mice were considered to contain chemoattractive factors (5, 46, 57, 65), we analyzed factors that induce hMSC migration by blocking experiments using antibodies against receptors for growth factors and chemokines and their ligands. To increase the accuracy of the interpretation of *in vitro* migration assays, we defined a ligand-receptor interaction as chemoattractive if antibodies against both the ligand and its cognate receptor reduced the migration of hMSCs. Based on this criterion, we expected that CCR3, CCR5, CXCR3, and CXCR4, and their ligands are possibly involved in the migration of hMSCs to the brain extracts of prion-infected mice (Fig. 2). The involvement of CXCL12/CXCR4 signaling in hMSCs migration is consistent with findings in hypoglossal nerve injury (24), ischemic (63), and glioma (11) models. Although an effect of CCR3, CCR5, or CXCR3

on MSC migration in brain injury has not been reported, CXCR3 and CCR5 are known to modulate resident microglial migration to brain lesions (6, 45). In prion diseases, impairment of microglial migration, associated with the increased accumulation of PrP^{Sc} but prolongation of survival, has been reported in CXCR3 gene deficient mice infected with prions (47). Microglial recruitment in retina after intraocular injection of homogenates from prion-infected neuroblastoma cells was inhibited by CCR5 antagonist, suggesting the involvement of CCR5 in microglial response to prion infection (34), although ablation of CCR5 gene did not influence the incubation period after prion infection (55). Since MSCs are able to migrate to brain lesions, the mechanisms by which they do so are expected to show some similarity with the mechanisms that underlie microglial migration. CCL2 has been reported to mediate MSC migration to ischemic brain lesions (62). However, neither an anti-CCL2 antibody, nor an antibody against its receptor, CCR2, reduced hMSC migration to brain extracts of prion-infected mice, implying that CCL2/CCR2 interaction may not mediate the migration of MSCs to prion-specific brain lesions. PDGF-AB and IGF-1 have been reported to be strong chemoattractants for MSC migration *in vitro* (42). In the present study, antibodies against these two growth factors reduced hMSC migration, but antibodies against their receptors did not inhibit hMSC migration despite the surface expression of these receptors on hMSCs (Fig. 4). Because of the complexity of the brain extracts and the limitations of blocking experiments, the lack of inhibition by these antibodies against those receptors does not necessarily mean that these ligand-receptor interactions have no functional relevance. Further detailed analysis will define additional factors that possibly mediate the migration of MSCs in response to damage of nervous tissue caused by prion propagation.

Regarding the expression of chemokine genes, the gene expression of CCR5 ligands (CCL3, CCL4, and CCL5), CCR3 ligands (CCL5 and CCL7), and the ligand for CXCR3 (CXCL10) was upregulated. The upregulation of CXCL10 gene in the CNS following viral infection has been reported to attract T lymphocytes bearing CXCR3 into the CNS (64), suggesting that MSCs share some mechanism of trafficking with lymphocyte trafficking. The hMSCs transplanted into the brains of mock-infected mice do not migrate, and the degree of hMSC migration in the brains of prion-infected mice correlates with the progression of neuropathological lesions (51). These results indicate that constitutive expression levels of chemokines and/or growth factors in the brain do not, but increased levels of those factors do, induce hMSC migration. Therefore, although CXCR4 and its ligand CXCL12 have been reported to play an important role in migration of MSCs in the CNS (24, 63), the lack of upregulation of CXCL12 gene expression in prion-infected mice suggests that CXCL12-CXCR4 interaction does not have an important role in the initial event on the attraction of hMSCs. Indeed, cell migration is dependent on a multitude of signals. Therefore, cytokines, chemokines, and growth factors, whose expression is upregulated in the brains of prion-infected mice, e.g., the CXCL10, CCL3 to CCL5, and CCL7 factors that we analyzed in the present study, as well as other factors reported previously (5, 57, 65), will stimulate hMSCs to initiate migration.

The corpus callosum is known to be one of the sites through which MSCs transplanted into one hemisphere migrate to the contralateral hemisphere (3, 19). We recently reported that hMSCs transplanted into the left thalamus of prion-infected mice were detected in the corpus callosum, the contralateral hippocampus and thalamus 2 days after transplantation (51). This result suggests that the hMSCs that were detected in the corpus callosum were migrating to the brain lesions in the contralateral hemisphere. Based on this idea, we therefore analyzed the expression of chemokine receptors on hMSCs that were transplanted into prion-infected mice. Interestingly, in agreement with the interpretation of the *in vitro* migration assays, hMSCs in the corpus callosum clearly expressed CCR3, CCR5, CXCR3, and CXCR4 2 days after transplantation (Fig. 5B), suggesting the involvement of these chemokine receptors in the migration of hMSCs *in vivo*. In contrast to hMSCs in the corpus callosum, hMSCs that had migrated to the contralateral hippocampus showed reduced expression of CCR3, CCR5, and CXCR3, whereas strong expression of CXCR4 was still observed. These results suggest that CXCR4 plays a role not only in migration but also in regulating hMSC activity following chemotactic migration. A role in the regulation of hMSC activity following chemotactic migration may also apply to the expression of CCR1 and CX3CR1; the weak expression of CCR1 and CX3CR1 on hMSCs in the corpus callosum (Fig. 5B) appears to be consistent with the results of the *in vitro* migration assay (Fig. 2). However, in contrast, these receptors were clearly expressed on hMSCs in the transplanted thalamus at 2 days posttransplantation and in the contralateral hippocampus of prion-infected mice a week after transplantation, implying that CCR1 and CX3CR1 may play a role in regulating MSC activity after migration to the targeted site.

Although neuroprotective functions of MSCs that have migrated to brain lesions are not fully understood, the temporal and spatial differences in the expression of chemokine receptors on hMSCs transplanted into the brains of prion-infected mice that we observed in the present study is intriguing, i.e., hMSCs that are considered to be in the process of migration in the corpus callosum expressed CCR3, CCR5, and CXCR3, whereas hMSCs that had migrated to the target site showed reduced expression of these receptors but elevated expression of CCR1 and CX3CR1. The stimulation of CX3CR1 by its ligand CX3CL1 plays a role in modulating the release of proinflammatory cytokines from microglia (7, 21) and in producing neuroprotective substances (31). Therefore, the expression of CX3CR1 on MSCs that had migrated to the contralateral hippocampus might be an indicator of functional alteration of hMSCs, i.e., alteration from active migration toward the target site to exhibition of neuroprotective potential. The hMSCs that had migrated to the contralateral hippocampus still expressed CCR1, CX3CR1, and CXCR4 at 3 weeks posttransplantation (data not shown). We have previously shown that hMSCs transplanted into prion-infected mice efficiently produced various neurotrophic factors at 1 to 3 weeks posttransplantation (51). It is thus conceivable that signaling via these receptors may facilitate alteration of the phenotype of hMSCs to that of a neuroprotective phenotype following chemotactic migration. The interaction between endogenous nucleotide and purinergic receptors on microglia is known to regulate the activation state of microglia. The interaction of ATP with the $P2Y_{12}$ receptor induces microglial chemotaxis to local CNS injury.